Atmos. Chem. Phys. Discuss., 12, 13237–13298, 2012
www.atmos-chem-phys-discuss.net/12/13237/2012/
doi:10.5194/acpd-12-13237-2012

Atmospheric Chemistry and Physics Discussions

New parameterization of dust emissions in the global atmospheric chemistry-climate model EMAC

M. Astitha[1], **J. Lelieveld**[1,3,4], **M. Abdel Kader**[1], **A. Pozzer**[2], **and A. de Meij**[1]

[1]Energy, Environment and Water Research Centre, The Cyprus Institute, Nicosia, Cyprus
[2]Earth System Physics Section, International Centre for Theoretical Physics, Trieste, Italy
[3]Max Planck Institute for Chemistry, Hahn-Meitnerweg 1, 55128 Mainz, Germany
[4]King Saud University, Riyadh, Saudi Arabia

Received: 30 April 2012 Accepted on – Accepted: 11 May 2012 – Published: 25 May 2012

Correspondence to: M. Astitha (m.astitha@cyi.ac.cy)

Published by Copernicus Publications on behalf of the European Geosciences Union.

Abstract

Airborne desert dust influences radiative transfer, atmospheric chemistry and dynamics, as well as nutrient transport and deposition. It directly and indirectly affects climate on regional and global scales. We present two versions of a parameterization scheme to compute desert dust emissions, incorporated into the atmospheric chemistry general circulation model EMAC (ECHAM5/MESSy2.41 Atmospheric Chemistry). One uses a globally uniform soil particle size distribution, whereas the other explicitly accounts for different soil textures worldwide. We have tested these schemes and investigated the sensitivity to input parameters, using remote sensing data from the Aerosol Robotic Network (AERONET) and dust concentrations and deposition measurements from the AeroCom dust benchmark database (and others). The two schemes are shown to produce similar atmospheric dust loads in the N-African region, while they deviate in the Asian, Middle Eastern and S-American regions. The dust outflow from Africa over the Atlantic Ocean is accurately simulated by both schemes, in magnitude, location and seasonality. The modelled dust concentrations and deposition fluxes compare well with observations at (island) stations in the Atlantic Ocean and Asia, and are underestimated in the Pacific Ocean where annual means are relatively low ($<1\,\mu g\,m^{-3}$). The two schemes perform similarly well, even though the total annual source differs by ~50 %, indicating the importance of transport and deposition processes (being the same for the two schemes). Our results emphasize the need to represent arid regions individually and explicitly in global models according to their unique land characteristics and meteorological conditions.

1 Introduction

Desert dust is an important atmospheric constituent, given its potential to affect air quality, nutrient deposition and climate (Sokilik and Toon, 1996; Tegen and Lacis, 1996; Ramanathan et al., 2001; Mahowald et al., 2005; Forster et al., 2007). Global models, being less dependent on boundary and initial conditions than limited area models, are useful tools to study the large-scale dynamics, the physico-chemical behaviour and deposition distributions of the dust aerosols. Furthermore, anthropogenic influences, including interactions between pollutant gases and aerosols with dust particles can be analysed, and their role in atmospheric chemistry and climate change simulated (Kallos et al., 2007; Astitha et al., 2010). The uncertainties associated with these processes and research questions are indicated by the large variety of global models using different emission parameterization schemes, input parameters and representations of aerosol removal processes (Ginoux et al., 2001; Tegen et al., 2002; Zender et al., 2003; Stier et al., 2005; Pringle et al., 2010). In many cases models are tuned towards the available observations, often performed at long distances from the main dust source areas. An important effort to compare the dust distributions from different global models, the Aerosol Comparisons between Observations and Models (AeroCom) project, has revealed a wide range of calculated global dust sources (514 to 4314 $Tg\,yr^{-1}$), deposition (676 to 5999 $Tg\,yr^{-1}$) and atmospheric burden (8.2 to 54 Tg) (Textor et al., 2006, 2007; Prospero et al., 2010; Huneeus et al., 2011), indicative of the uncertainties involved.

Mineral dust particles enter the lower atmosphere primarily through a mechanism called saltation bombardment, which is strongly dependent on the meteorological conditions near the surface, as well as the soil texture and particle size classification (Shao et al., 1993; Alfaro and Gomes, 2001; Grini et al., 2002). Thus, the emissions of dust particles have important consequences on a global scale, whereas the phenomenon itself is of episodic nature driven by processes on small spatial and temporal scales. Therefore, global models need to be based on a number of assumptions to simplify and generalize the dust emission schemes. Several methods have been proposed to estimate the dust flux into the atmosphere, some more detailed than others (Marticorena and Bergametti, 1995; Marticorena et al., 1997; Shao et al., 1993, 2004, 2011; Alfaro and Gomes, 2001; Nickovic et al., 2001; Tegen et al., 2002; Zender et al., 2003; Balkanski et al., 2004). In most cases a physics-based dust emission scheme is pursued that

ACPD
12, 13237–13298, 2012

explicitly takes into account the soil surface characteristics. One of the limitations in a global setup involves the availability of input parameters for which measurement data are lacking. While this applies to both global and regional models, detailed datasets have been collected of soil characteristics for specific desert areas (Callot et al., 2000; Laurent et al., 2005, 2006, 2008), and regional models are typically more sophisticated in representing dust emissions. Further, the difficulty of directly measuring the dust emission fluxes in the source areas hinders the evaluation of model results.

The goal of our study is to develop and test two versions of a new dust emission parameterization, implemented into the atmospheric chemistry – general circulation model EMAC (Jöckel et al., 2005, 2006, 2010; Roeckner et al., 2006), and overcome some of the above mentioned limitations and difficulties. We address (i) the physical processes that lead to the injection of dust particles into the atmosphere and (ii) the role of the input parameters in representing the spatial heterogeneity of dust emissions. One advantage of using EMAC is the direct coupling to meteorological calculations at each time step (10 min), which is expected to realistically represent the grid-scale temporal variability, e.g., compared to off-line calculations with a chemistry-transport model based on 3- or 6-hourly meteorological analyses. We thus combine the meteorological variables with specific input fields of soil properties, and without using a-priori (or preferential) sources distributions of dust or pre-calculated tables of input variables.

The paper is organized in five sections. The next section describes the EMAC model and the configuration used for the simulations. In Sect. 3, the dust production scheme is presented and analysed considering the two different implementations. The observational data, collected for the comparison with the model results, is discussed in Sect. 4, which includes in-situ measurements from the AeroCom dust benchmark dataset (Huneeus et al., 2011; Perez et al., 2011) and remote sensing data. In Sect. 5 the effects of nudging the model to meteorological analyses are discussed, and an extensive model evaluation with sub-sections on concentrations, deposition fluxes and aerosol optical depth presented. A discussion about the differences between the two versions of the parameterization is also included.

ACPD
12, 13237–13298, 2012

2 EMAC model configuration

The EMAC model combines the ECHAM5 general circulation model (Roeckner et al., 2006) and the Modular Earth Submodel System (Jöckel et al., 2005, 2006, 2010). The MESSy system (version 2.42) is modular and all sub-models follow strict coding standards to allow easy implementation within other models. This provides the option of running the model with multiple representations of processes to systematically test and improve the results. The model was run with a spectral resolution of T106 ($\sim 1.1^{\circ} \times 1.1^{\circ}$) and 31 vertical levels up to 10 hPa for the year 2000. The reason for selecting this year is the availability of ample dust measurement data, important for the evaluation procedure. Glaser et al. (2011) used four horizontal resolutions, with T106 being the highest, and concluded that important differences occur in the dust emissions, which are not well described in the coarser resolution setups. The model output is recorded every 5 h providing an entire daily cycle (1 h resolution) after 5 days. The simulations performed include a simplified sulphur chemistry scheme allowing the production of sulphuric acid and particulate sulphate, which play an important role in transforming the dust particles from hydrophobic into hydrophyllic, thus affecting their ability to interact with clouds and be removed by precipitation. More details on the sulphur chemistry mechanism and the set of chemical reactions can be found in Glaser et al. (2011). The aerosol microphysics sub-model is M7 (Vignati et al., 2004; Stier et al., 2005), which describes the aerosol size distribution according to 7 lognormal modal size fractions; 4 soluble and 3 insoluble, encompassing the nucleation, Aitken, accumulation and coarse modes.

The emissions of gases and aerosols are treated using online and offline routines and the processes taken into account in the simulations include convection, deposition (wet and dry) and radiation, among others. The set of sub-models activated in the EMAC version are described in Table 1, including references to the original work. The following emission sub-models are used: (a) the fixed (offline) emissions include sulphur dioxide from anthropogenic, volcanic sources and biomass burning; nitrogen ox-

ACPD
12, 13237–13298, 2012

ide from anthropogenic, aircraft, biogenic sources and biomass burning; black carbon and organic carbon from wildfires; dimethyl sulphide from terrestrial sources; formaldehyde, formic acid and methanol from anthropogenic sources and biomass burning. (b) The online emissions include dimethyl sulphide from water bodies, nitrogen oxide from soil biogenic sources, organic and black carbon (bio-fuel, fossil fuel, and secondary species), dust and sea salt. The present work extends this scheme with mineral dust sources.

The model performance of simulating the global dust distribution was also tested using the nudging option, in contrast to the free-running mode. As pointed out by Timmreck and Schulz (2004), significant differences can occur between nudged and free-running simulations, in particular with respect to the mean geographical distribution and seasonal variability of mineral dust. For the nudged simulations the European Centre for Medium-Range Weather Forecasts (ECMWF) 40-yr re-analysis (ERA-40) data for the year 2000 has been used. The prognostic variables nudged towards the observations (i.e., the re-analyses) are temperature, vorticity, divergence and surface pressure, and the nudging weights are chosen such that the boundary layer and the upper troposphere/lower stratosphere are not directly influenced (Lelieveld et al., 2007). A discussion about the effects of nudging on the simulated dust concentrations and deposition is included in Sect. 5.

3 Dust emission parameterization

The previous dust emission scheme in the EMAC model was based on the work of Balkanski et al. (2004) as discussed in Stier et al. (2005). It includes three pre-calculated tables of clay content, emission source strength factors ($\mathrm{kg\,s^2\,m^{-2}}$) and threshold wind friction velocities ($\mathrm{m\,s^{-1}}$), representing the entire globe. The modelled temperature and precipitation fields are used to adjust the soil wetness and thus limit the dust production in wetted soil areas. The vertical dust flux (only coarse dust particles were emitted) was calculated with the use of the diagnosed wind speed at 10 m,

Discussion Paper | Discussion Paper | Discussion Paper | Discussion Paper |
ACPD
12, 13237–13298, 2012
New parameterization of dust emissions in EMAC
M. Astitha et al.

the threshold velocity and the emission source strength factor from the pre-calculated tables. The results of the Balkanski dust emission scheme are also discussed in Glaser et al. (2011), comparing it with the Tegen et al. (2002) scheme recently implemented in the EMAC model.

The methodology followed in this work is based on previous dust emission schemes for regional (Perez et al., 2006; Spyrou et al., 2010; Laurent et al., 2008, 2010; Marticorena et al., 1997) and global modelling systems (Zender et al., 2003; Tegen et al., 2002). Two versions of our dust emission parameterization have been included into EMAC, presented in detail in the following sub-sections.

3.1 Dust sources and input parameters

Dust particles are injected into the atmosphere through saltation and sandblasting (Marticorena and Bergametti, 1995; Marticorena et al., 1997; Grini et al., 2002; Zender et al., 2003). The saltation process is initiated when the drag near the surface exceeds the gravitational inertia of the sand-size particles (diameter > 60–80 µm) moving them downwind horizontally. With this movement the large particles disaggregate and release smaller size silt and clay particles (sandblasting) (Grini et al., 2002; Alfaro and Gomes, 2001). The height of the saltation layer is of the order of 1 m, which underscores that the dust emissions take place on small spatial scales. The direct emission of small and coarse dust particles, referred to as aerodynamic entrainment (Shao, 2004; Shao et al., 2011), is negligible because of cohesive and gravitational forces, respectively, which bind the particles to the soil; this mechanism is not included here considering the negligible contribution compared to saltation bombardment. A third mechanism of dust entrainment into the atmosphere is disintegration (self-abrasion) of large aggregates or fragments (Shao et al., 2011), which is considered difficult to model on a global scale due to the lack of input data that characterize the aggregates in the soil. The dust particles are considered to be mobilized in the atmosphere when the wind friction velocity, a proxy of the surface drag properties, exceeds a threshold value.

ACPD
12, 13237–13298, 2012

This threshold value depends on the soil size distribution and soil texture classification. Details on the calculation of the threshold friction velocity are given in Sect. 3.2.

For the new implementation two formulations of the online dust production are tested, from here on referred to as DU1 and DU2. DU1 utilizes a homogeneous global soil size distribution of dust particles and DU2 uses an explicit geographical representation instead. The input parameters that both emission schemes have in common are described below. One of the first important input parameters is the location of the dust sources. Both formulations use as input fields the geographical sources of dust based on the Olson global ecosystem biomes (Olson, 1992) as described in Table 2. This database provides global information on the location of deserts (sand or clay), semi-deserts (steppe, shrub, sparse grass) and flat desert playas (Fig. 1, left plot). The set of input parameters also includes the clay fraction of the soils (Scholes and Brown de Colstoun, 2011) as shown in Fig. 1, right plot, the rooting depth (Schenk and Jackson, 2009) and the monthly vegetation area index (sum of leaf and stem area index) as discussed in Zender et al. (2003). The schemes use the online meteorological fields from the EMAC model: temperature, pressure, relative humidity, soil moisture and the surface friction velocity. Each relevant parameter will be discussed in the following subsections.

3.2 Threshold friction velocity

A central part of the dust production scheme is the calculation of the threshold friction velocity (u_{*thr}), above which the emission of dust particles into the air is considered possible. It is based on an empirical relationship derived by Marticorena and Bergametti (1995) and analyzed in Marticorena et al. (1997) over smooth surfaces based on the proposed formulations of Iversen and White (1982). The relationship utilizes the friction Reynolds number B, which depends on the soil particle size D_p, in Eqs. (1–3). This relationship indicates that the minimum threshold friction velocity occurs for soil particle diameters around 60–70 µm (Fig. 2a).

$$\left.\begin{array}{ll} u_{*ts}(D_p) = \frac{0.129\mathrm{K}}{\sqrt{1.928B^{0.092}-1}} & 0.03 < B < 10 \\ u_{*ts}(D_p) = 0.129\,\mathrm{K}[1-0.0858\exp(-0.0617(B-10))] & B > 10 \end{array}\right\} \quad (1)$$

$$\text{where}\quad K = \sqrt{\frac{\rho_p g D_p}{\rho_\alpha}\left(1+\frac{0.006}{\rho_p g D_p^{2.5}}\right)}$$

$$B = \frac{u_{*ts} D_p}{v} \quad (2)$$

$$B = 1331 D_p^{1.56} + 0.38 \quad \text{empirical analytical solution} \quad (3)$$

where u_{*ts} is the threshold friction velocity over smooth surfaces, D_p is the diameter of the soil particle, v is the kinematic viscosity of air, ρ_p is the particle density, ρ_α is the air density and g the gravitational acceleration. The above Eqs. (1–3) are implemented in the first version of the dust emission scheme (DU1), with the iterative Eq. (2) being used in the second timestep whereas the analytical solution Eq. (3) is used at the start of the calculation. The difference with the DU2 scheme is that in DU1 the D_p is constant and equal to the optimal diameter for saltation (60 µm), when in DU2 the soil size distribution is included as an input field, and the threshold wind friction velocity is calculated for particle diameters in the range of 0.1 to 1000 µm.

Two corrections are imposed in the calculated u_{*ts} which are related to the drag partition scheme near the surface (Marticorena et al., 1997) and the soil moisture (Fecan et al., 1999). Since the initial computation of the u_{*ts} is an empirical relation for smooth surfaces, a correction is imposed depending on the surface roughness length (z_o) and the local roughness length of the uncovered surface (z_{os}). The empirical relation is shown in Eq. (4) and it is valid for small values of aeolian roughness ($z_o < 1$ cm) (Darmenova et al., 2009). An example of how the correction factor ($1/f_{drag}$ is the multiplication factor for u_{*ts}) changes with the surface roughness length z_o and local roughness

ACPD
12, 13237–13298, 2012

New parameterization of dust emissions in EMAC

M. Astitha et al.

length z_{os} is given in Fig. 2b. As shown in the graph, the correction factor is higher for higher z_o and lower z_{os}, which leads to higher values of u_{*thr} (Eq. 5). The reason for this is that a higher threshold friction velocity must be assigned for a surface with more obstacles. When the soil includes an increased number of non-erodible elements (solid obstacles, i.e. rocks, pebbles, vegetation), which translates into higher values of z_o, the threshold friction velocity increases causing a decrease in the emission of dust particles. When z_{os} increases (i.e., smoother surfaces) the correction factor decreases ($1/f_{drag}$), giving smaller values of u_{*thr}.

$$f_{drag} = 1 - \frac{\ln \frac{z_o}{z_{os}}}{\ln \left[0.35 \left(\frac{10}{z_{os}}\right)^{0.8}\right]} \quad (4)$$

$$u_{*thr} = \frac{u_{*ts}}{f_{drag}} \quad (5)$$

For both dust emission schemes DU1 and DU2, globally uniform values have been used for z_o and z_{os} (0.01 and 0.00333 cm, respectively, as in Zender et al., 2003).

The final correction in the calculation of the threshold friction velocity is the soil moisture adjustment as proposed by Fecan et al. (1999) and applied by Marticorena et al. (1997) and also Zender et al. (2003), Laurent et al. (2005, 2006, 2008), among others. The principle behind this correction is that the threshold friction velocity must increase in wetted soils and this is accomplished by relating the residual soil moisture to the clay content of the soil. The residual soil moisture w is calculated with the empirical Eq. (6), and its physical meaning is given as the ratio of the mass of water to the mass of dry soil:

$$w' = 0.0014(\%\ \text{clay})^2 + 0.17(\%\ \text{clay}) \qquad \text{residual soil moisture} \quad (6)$$

Besides the residual soil moisture, the soil moisture correction scheme requires the gravimetric soil moisture w, which is calculated from the modelled soil moisture w_s (m)

ACPD
12, 13237–13298, 2012

by dividing with the rooting depth (Hillel, 1980). The final correction of the threshold friction velocity is calculated based on Eq. (7), depending on whether the soil is dry or wet.

$$\begin{aligned} u_{*t} &= u_{*thr} && \text{for } w < w' (\text{dry soil}) \\ u_{*t} &= u_{*thr}\sqrt{1 + 1.21(w - w')^{0.68}} && \text{for } w > w' (\text{wet soil}) \end{aligned} \tag{7}$$

Both emission schemes DU1 and DU2 use the above soil moisture correction in the formulation of Eqs. (6) and (7), since it is not dependent on the soil size distribution. The sequence described above provides the threshold friction velocity u_{*t} that enters the calculation of horizontal and vertical fluxes, as discussed in the following subsection.

3.3 Horizontal and vertical flux calculations

The final step is the calculation of horizontal (H) and vertical (V) fluxes of the dust particles entering the atmosphere. Following Marticorena et al. (1997) the horizontal flux is calculated with Eq. (8) or (9), depending on whether or not the soil size distribution is accounted for:

$$H = \frac{c\rho_{air}u_*^3}{g}\left(1 + \frac{u_{*t}}{u_*}\right)\left(1 - \frac{u_{*t}}{u_*}\right)^2 \quad \text{when} \quad u_* > u_{*t} \tag{8}$$

$$H(D_p) = \frac{c\rho_{air}u_*^3}{g}\left(1 + \frac{u_{*t}(D_p)}{u_*}\right)\left(1 - \frac{u_{*t}(D_p)}{u_*}\right)^2 S_{rel}(D_p) \quad \text{when} \quad u_* > u_{*t} \tag{9}$$

where $c = 1$ (Darmenova et al., 2009), ρ_{air} is the air density, u_* is the friction velocity, u_{*t} is the threshold friction velocity, S_{rel} is the relative surface area covered from particles with diameter D_p (assuming particles of spherical shape).

In DU1 the horizontal flux is calculated using Eq. (8) (Zender et al., 2003; Spyrou et al., 2010), since there is no size distribution assigned to the soil particles. In DU2, Eqs. (9) and (10) are implemented to estimate the horizontal flux per soil particle of size D_p and the total horizontal flux per soil source i, $H_{tot,i}$.

ACPD
12, 13237–13298, 2012

The vertical flux V is defined as the mass of dust particles emitted from unit area per unit time ($\mathrm{kg\,m^{-2}\,s^{-1}}$). V is considered proportional to the horizontal flux H and is calculated by the relationship $V = a \cdot H$, where a is the sandblasting efficiency that depends on the clay content of the soil. In this formulation the empirical relationship of Marticorena and Bergametti (1995) is adopted:

$$a = 10^{0.134(\%\ \mathrm{clay})-6} \tag{10}$$

Equation (10) is valid for clay percentages up to 20 %. For higher clay contents the sandblasting efficiency is set constant to the values proposed by Tegen et al. (2002). Specifically:

$$a = 1.0 \times 10^{-6}\,\mathrm{cm}^{-1} \quad \text{for} \quad 20 \le (\%\ \mathrm{clay}) < 45$$
$$a = 1.0 \times 10^{-7}\,\mathrm{cm}^{-1} \quad \text{for} \quad (\%\ \mathrm{clay}) \ge 45$$

The final equation that provides the dust vertical flux V for both DU1 and DU2 is described in the following subsection, in which we discuss the particle size distribution, which is stated to be of central importance by Kok (2011).

3.4 Soil and transport size distributions

The main difference between the two implementations involves the soil size distribution characterization. In the DU1 version of the scheme we adopt an optimum size for saltation of $D_o = 60\,\mu\mathrm{m}$ at which the threshold friction velocity has a minimum (Marticorena and Bergametti, 1995; Spyrou et al., 2010). It assumes that all erodible regions contain particles of size D_o so that saltation is initiated when the friction velocity exceeds the threshold at D_o. Thus, the threshold friction velocity and the horizontal flux H are calculated without a dependency on soil particle size. To estimate the dust vertical flux V distributed over particle sizes, the soil size distribution at the sources is assumed to follow a tri-modal distribution based on the "background" modes suggested by D'Almeida (1987) and used in Zender et al. (2003). This source size distribution is considered

ACPD
12, 13237–13298, 2012

globally uniform and the parameters of the distribution are as follows: mass median diameters $D_v = 0.832$, 4.82, 19.38 and geometric standard deviation $\sigma_g = 2.10$, 1.9, and 1.6, followed by the mass fraction of each mode: $m_i = 0.036$, 0.957, and 0.007, respectively.

The size distribution of the soil elements is different from the size distribution of the particles set in motion into the atmosphere. Once the particles are emitted into the air, the particle size distribution is adjusted to the 8 size bin modes from 0.2 to 20 µm in diameter after Perez et al. (2006). Because the mass in the source modes is log-normally distributed, the mass fraction overlap M_{ij} of each source mode i, carried in each transport bin j, is calculated with the use of the standard error function (Schulz et al., 1998; Zender et al., 2003):

$$M_{ij} = \frac{1}{2}\left[\operatorname{erf}\left(\frac{\ln(D_{\max,j}/D_{v,i})}{\sqrt{2}\ln\sigma_{g,i}}\right) - \operatorname{erf}\left(\frac{\ln(D_{\min,j}/D_{v,i})}{\sqrt{2}\ln\sigma_{g,i}}\right)\right] \quad (11)$$

where $D_{\min}$ and $D_{\max}$ are the minimum and maximum diameters of each transport bin j, and D_v is the mass median diameter of the source i.

Finalizing the formulation of the dust emissions scheme DU1, the vertical flux ($\mathrm{kg\,m^{-2}\,s^{-1}}$) for each transport bin j, is calculated using:

$$V_j = F_1 B\alpha H \sum_{i=1}^{3} m_i M_{i,j} \quad (12)$$

where F_1 is an empirical conversion factor (10^{-4} for DU1), B is the fraction of bare soil exposed in a grid cell (depends on the percentage of each Olson biome, the fraction of land covered by water or snow and the fraction of ground covered by vegetation; the vegetation area index is used to calculate the monthly fraction of ground covered by vegetation), α is the sandblasting efficiency, H is the horizontal flux and $\sum_{i=1}^{3} m_i M_{i,j}$ is the mass fraction of each transport bin.

Discussion Paper | Discussion Paper | Discussion Paper | Discussion Paper |

ACPD
12, 13237–13298, 2012

New parameterization of dust emissions in EMAC

M. Astitha et al.

In the second scheme DU2, an explicit size distribution of the soil is introduced, based on the Zobler soil type categorization, thus representing each grid cell by fractions of defined particle sizes (7 types from coarse to fine organized in 4 modes as shown in Tegen et al. (2002), and shown in Table 3). The mass fraction mf_i of each size population is also listed in Table 3. As in DU1, the transport size distribution is adjusted to 8-size bins from 0.2 to 20 µm in diameter. The horizontal dust flux is calculated with equation 9 for each diameter of the soil particles (ranging from 0.1 to 1000 µm) and equation 10 for the total horizontal flux of each source ($i = 1$ to 4). Consequently, the vertical flux V for every transport bin is estimated as follows:

$$V_j = F_2 B \alpha H_{\mathrm{tot}} M_j \tag{13}$$

where $M_j = \sum_{i=1}^{4} \mathrm{mf}_i M_{ij}$

The parameters in Eq. (13) are the same as described in Eq. (12), with the exception of the empirical conversion factor ($F_2 = 10^{-3}$ for DU2), H_{tot}, which corresponds to the total horizontal flux for each grid cell and mf_i, which is the mass fraction of each of the four source sizes in Table 3.

For consistency with the aerosol module in the EMAC model, the 8 transport size bins are grouped into the accumulation and coarse insoluble modes used for all aerosol physical and chemical processes (the Aitken mode is not produced by the dust scheme). The aerosol module used in this work is M7 (Vignati et al., 2004), using 7 size modes for the aerosol distribution. The freshly emitted dust particles are assumed to be initially insoluble, with a geometric standard deviation and mass median diameter $\sigma_g = 2$, mmd = 3.5 µm for the coarse mode and $\sigma_g = 1.59$, mmd = 0.7 µm for the accumulation mode (Cheng et al., 2008). The differences between the two versions of the dust emission scheme (DU1 and DU2) are summarized in Table 4.

ACPD
12, 13237–13298, 2012

4 Observational data

For the comparison with model results, available observational datasets of monthly and annual dust concentrations and deposition, aerosol optical depth from sun-photometer data include those of the Aerosol Robotic Network (AERONET), and additionally from the MODIS-Terra (v5.1 – Level 3 product), MISR-Terra (v.31 – Level 3 product) satellite instruments and Deep Blue algorithm. The concentration and deposition datasets are taken from the AeroCom benchmark dataset presented by Huneeus et al. (2011) (N. Huneeus, personal communication, 2011). More specifically, the comparison is performed for monthly and annually averaged dust concentrations based on measurements at 24 stations, of which 22 are managed by the Rosenstiel School of Marine and Atmospheric Science, University of Miami (Prospero et al., 1989; Prospero, 1996; Arimoto et al., 1995). Two additional stations, Jabirun and Ruchomechi, are added as in Huneeus et al. (2011). All measurement stations are located downwind though remote from the main dust source areas, and the measurement period covers the 1980s and 1990s, while each station has been active during different periods.

The dust concentrations are derived from measured aluminium concentrations assuming an Al content of 8 % in soil dust (Prospero, 1999) or from the weights of filter samples ashed at 500 °C after extracting soluble components with water as described in Huneeus et al. (2011). Figure 3a shows the locations of the 24 stations; the names and coordinates are given in Table S1 of the Supplement. From this dataset we also use the annual average from each station to evaluate the model calculated annual and seasonal dust distributions. These measurements are multi-annual and not for the simulation year 2000, which will be taken into account in the model evaluation in Sect. 5.1. Furthermore, monthly dust concentration measurements for 2000 are available for Miami and Barbados (J. Prospero, personal communication, 2010) and for Tel Shikmona (Haifa, Israel) (B. Herut, personal communication, 2012).

The deposition of dust particles directly relates to their distribution and mass load in the atmosphere. Dust particles are mostly deposited through precipitation scavenging

ACPD
12, 13237–13298, 2012

and sedimentation and to a lesser extent through dry deposition. Annual deposition data from 84 sites (names and locations are listed in Table S2 of the Supplement) are used to evaluate the modelled dust deposition. This dataset is a collection from different sources, the measurement period being different for the stations; for more details we refer to the indicated publications. The 84 stations are shown in Fig. 3b, colour-coded according to region. The regions are: Europe, Asia, N- and S-Atlantic, S- and W-Pacific, S-Ocean and Indian Ocean (Table S2, Supplement). Further, the monthly dust masses deposited in three locations in Florida are used (Florida Atmospheric Mercury Study-FAMS network; Prospero et al., 2010). The deposition measurements for each site have been averaged by month over three years (1994–1996), providing the total and the wet deposition fraction. More details on these datasets can be found in Huneeus et al. (2011).

The AOD observed by the AERONET stations (level 2 data) is used to compare with the model output for the year 2000 on a daily, monthly and annual basis. The modelled AOD is calculated at 550 nm using concentrations of dust and sea salt particles and biomass burning products (black carbon and organic carbon). The anthropogenic fraction of the aerosol species is not relevant, since the simulation does not include a full chemistry scheme but a simple sulphur chemistry alternative. Since the AERONET AOD is rarely given at 500 nm or 550 nm, the measured AOD at 550 nm is extracted by an interpolation method using the measurements at 440 and 870 nm (de Meij and Lelieveld, 2011). The AERONET stations provide AOD data during daytime and clear sky conditions, and the daily average of the available measurements is used for the evaluation.

The selection of the AERONET stations included in this evaluation presupposes that they are located in areas influenced mainly by dust sources, thus excluding highly polluted regions. To select the appropriate stations for the year 2000, two criteria were applied to the daily AOD of each available station. The first criterion is that the $AOD_{550\,nm}$ exceeds 0.2 and the second that the Angstrom exponent ($AE_{500–870\,nm}$) is less than 1.2 to select the coarser particles associated with desert dust transport. The station is

ACPD
12, 13237–13298, 2012

considered “dusty” if at least 20 % of the available data satisfies the above criteria. This methodology has provided 19 available stations for the simulation year 2000. A list is presented in Table S3 of the Supplement and the location of each station is shown in Fig. 3d. For some stations the availability of the AERONET aerosol optical depth has been limited and in these cases monthly AOD values from MODIS-Terra, MISR and MODIS Deep Blue have been included to evaluate the model. Of course, there are limitations in the use of level-3 data, which are averages from level-2 pixels on a 1 × 1 degree resolution. The sampling of actual retrievals is highly non-uniform in space and time, even at the resolution of these products (MODIS 1 × 1 degree and MISR 0.5 × 0.5 degree) (Kahn et al., 2009). The use of the satellite data is complementary to that of the AERONET data, since it is not recommended to draw strong conclusions based on level 3 data products.

5 Results

5.1 Effects of nudging to meteorological analyses

As discussed in Timmreck and Schulz (2004), nudging a simulation with observed, i.e., analysed meteorological data compared to a free-running general circulation model, can substantially affect the simulated global dust budget and, e.g., the seasonal variability of concentration distributions. In this work, the ERA40 reanalysis data has been assimilated into EMAC for the nudged simulation, and as a second option the free-running model was used by applying multi-annual mean sea surface temperatures and ice coverage as boundary conditions. The latter runs were included to study possible artefacts by the nudging and differences relevant for climate change applications. The simulations are denoted as DU1 and DU2 for the free-running model and DU1_ERA40 and DU2_ERA40 for the nudged model. At first glance the differences in the annual emissions from running the model in these two modes are hardly discernible (Fig. 4, comparing upper to lower panels). The geographical distribution is largely the same,

ACPD
12, 13237–13298, 2012

except for some areas where the emission flux appears to be lower in the nudged simulation (N-Africa, Arabian Peninsula). By calculating the global emission fluxes the differences become more apparent (Table 5).

The nudged simulations (DU1_ERA40 and DU2_ERA40) produce less dust globally compared to the free-running model, in agreement with the results of Timmreck and Schulz (2004) for the ECHAM4 climate model, indicating that the nudging somewhat reduces the wind speed and the dust emissions accordingly. For DU1, the reduction of the annual emissions is ~ 20 % and for DU2 it is ~ 24 %. The atmospheric lifetime of airborne dust is slightly longer in the nudged version of the model. The annual deposition reduces in line with the emissions between 16 and 25 %, and the annual atmospheric loads are also reduced compared to the free-running model (−14 % for DU1 and −19 % for DU2). The parameterization of the dust emissions is such that even small differences in the friction velocity can have substantial effects (Eqs. 8 and 9 include a dependency of the horizontal flux on the friction velocity to the power of three). The same is evident from the regional analysis of the dust budgets in Table 6. The nudged simulations produce lower emissions compared to the free running model in all areas except Australia, probably because the wind speeds are less affected there by the nudging (Fig. S1 in the Supplement demonstrates the seasonal difference in the emissions for DU1 and DU1_ERA40).

In spite of the effects of the nudging on the dust emission strength, its importance for a direct comparison with observations is illustrated in Fig. 5, showing model results and measurement data at the station Miami (courtesy J. Prospero). This station is affected by dust transport from the Sahara, predominantly in summer, whereas during winter the predominantly westerly winds prevent such transports. The lower panel shows the multi-year mean simulation, indicating that the seasonal cycle is captured well by the free running model in a statistical sense. The upper panel shows the comparison for the year 2000, indicating a bimodal seasonal profile, thus deviating from the multi-annual mean. Again the model seems to capture the seasonality well, suggesting that the

ACPD
12, 13237–13298, 2012

Title Page
Abstract | Introduction
Conclusions | References
Tables | Figures
◀| |▶
◀ ▶
Back | Close
Full Screen / Esc
Printer-friendly Version
Interactive Discussion

statistics can be reproduced without accounting for actual meteorological conditions, whereas the simulation of the year 2000 is clearly more realistic.

5.2 Evaluation of model results

5.2.1 Dust concentrations

Figure 6 presents a comparison of the annual mean dust concentrations calculated for the year 2000 and the observed multi-annual means at 24 stations. The model appears to simulate the spatial variability with both emission parameterization schemes DU1 and DU2 reasonably well. The colours of the symbols in Fig. 6 correspond to the station locations shown in Fig. 3a, to help distinguish the geographical areas. The same colour coding is used throughout this section. The month of January is excluded to avoid differences due to the model initialization. The comparison for stations in the Atlantic region (Barbados, Izana, Bermuda, Miami and Mace Head shown in green) indicates good agreement for all simulations (DU1, DU2, DU1_ERA40 and DU2_ERA40), i.e., quite close to the 1:1 relationship. This demonstrates the ability of the model to simulate the transport of dust from the main source areas in N-Africa. The simulations for the Asian stations (Cheju and Hedo in pink) are also in good agreement with the observed annual means, with the highest correlation for the DU2 and DU2_ERA40 model versions. By also considering Midway Island (no. 12 in Fig. 3a) as a station predominantly affected by Asian desert dust transports, the correlation with the observed values is close to 1:1 in the DU2 simulation. This contrasts with the findings of Huneeus et al. (2011) for most of the global models. For the S-Ocean stations (grey) the model overestimates the dust concentrations at two of the three stations (Marsh and Palmer) and underestimates it at the third (Mawson in Antarctica). The results nevertheless lie to a large extent within the 1:10 and 10:1 range for most of the simulations. For the two stations in S-Africa (blue), which are influenced by the Kalahari Desert, the comparison is not conclusive, since at one station the model overestimates (Cape Point) and at the other it underestimates (Rukomechi) the dust concentrations. The Pacific Ocean

ACPD
12, 13237–13298, 2012

stations (orange and red) appear to be the most problematic since different results are obtained for each of the simulations, though the model generally underestimates the observed concentrations. Interestingly, these are stations with annual average concentrations below 1 µg m^{-3}. Huneeus et al. (2011) found that many global models have difficulties representing dust concentrations at such locations. Finally, the dust observed in Australian stations (yellow), i.e., Cape Grim and Jabirun, is underestimated by all simulations.

The statistical analysis, comparing the annual average dust concentrations from multi-annual observations to the model results for the year 2000, indicates overall good agreement (Table 7). The correlation coefficient is in the range 0.84–0.88 and the bias is relatively low, especially for the nudged simulations. The root mean square error (RMSE) is lowest for the nudged simulations, for which the linear regression is closest to one. The difference between the simulations is generally small, although the nudged run using the DU2 version of the dust scheme (DU2_ERA40) slightly outperforms the other model versions.

Extending the comparison for these 24 stations to the monthly average dust concentrations, the general picture is similar (Fig. 7). Again, January has been excluded. The simulation results for the Atlantic Ocean stations (green) correlate rather well with the observations in all simulations, though there are some exceptions. These involve, e.g., the months March and October for the stations Mace Head, Bermuda and Miami, where the modelled dust concentrations are significantly too low. This also applies to July in Mace Head, and to September and November in Bermuda. The monthly mean model results at the Asian stations (pink) agree well with the observations, in line with the annual averages. The modelled dust concentrations over the Pacific Ocean stations (orange and red) are again underestimated by all simulations, in line with the results for the annual means mentioned above (< 1 µg m^{-3}). The comparison for the S-Ocean stations indicates best agreement between the DU1_ERA40 results and the observations, though an overestimation is evident for all simulations. The statistical analysis shows that the comparison is generally best for the DU2_ERA40 nudged simulation

ACPD
12, 13237–13298, 2012

with a correlation coefficient of 0.54, a linear regression close to one and the smallest RMSE (Table 8). Nonetheless, it appears that the model generally underestimates dust concentrations, notably in locations where concentrations are relatively low. This may indicate that removal processes during transport may generally be too efficient, possibly related to the solubility and the wet removal of dust particles.

Dust concentration measurements for the year 2000 were kindly provided for 3 stations (Barbados, Miami, USA, and Tel Shikmona near Haifa, Israel) by J. Prospero (personal communication, 2010) and B. Herut (personal communication, 2012), respectively. The availability of these important datasets, together with AERONET data, has motivated our selection of the year 2000 for the simulations. Figure 8 compares the observations to the results of the nudged simulations, and the agreement is generally satisfactory though not ideal. The two parameterizations give similar results for Barbados and Miami (Fig. 8 upper and middle plot, respectively), with the Barbados concentrations being overestimated by the model and the Miami ones matching relatively well. In Barbados the model overestimates concentrations during the dusty summer season, especially in August. In Miami concentrations agree well in this season though the model underestimates concentrations in the transition seasons, especially in September–October. For the Tel Shikmona station, the DU1 scheme appears to perform better than DU2, though the differences are not large. During two days in April (11–12) the model results are substantially higher than the observations, i.e., with both versions of the parameterization scheme, which may be related to the meteorological conditions in that period. For all three stations the correlation coefficients are rather high (0.73–0.91) and the spread in the scatter plots is low.

5.2.2 Dust deposition

Annual deposition measurements of dust are available for 84 stations, and monthly bulk and wet deposition dust data for three locations in Florida, as mentioned in Sect. 4. The 84 stations are shown in Fig. 3b, and are typically located downwind and partly remote from the main dust source areas. This implies that to a large degree we test the trans-

ACPD
12, 13237–13298, 2012

port and deposition qualities of the model, and to a lesser extent the emission schemes, depending on the distance from the sources. The data represent multi-annual averages that unfortunately do not match the simulation year. The comparison with the different simulations is shown in the scatter plots of Fig. 9, which also includes correlation coefficients, biases and RMSEs. Again, the colour of the data points in the scatter plots relates to the location of the stations shown in Fig. 3b.

The deposition over Atlantic Ocean stations (green) is very well reproduced by the model in all four simulations, in line with the above described evaluation, indicating that the dust outflow from N-Africa over the Atlantic Ocean is accurately simulated. Dust deposition in the E- and W-Pacific locations (red and orange) tends to be underestimated by the model, though the DU2 version substantially improves the simulation for the E-Pacific region. The modelled deposition over the S-Ocean (grey) is overestimated in some locations, while indicating higher correlations with observations in the DU1_ERA40 simulation. The modelled deposition over the Indian Ocean (black) and at European stations (blue) agrees reasonably well with the observations. Only for one location at the Taklimakan desert in Central Asia (purple) and one in the Middle East (brown) the model systematically underestimates the dust deposition. The statistical analysis of the four simulations shows that the bias and RMSE are lowest and the correlation highest for the DU2 simulation, while the DU2_ERA40 simulation results are actually quite similar.

Measurements of bulk and wet deposition at three locations in Florida during three consecutive years (1994–1996) have been used to additionally evaluate the dust deposition simulations and also to assess the contribution of wet deposition. The stations are Lake Barco, Tamiami Trail and Little Crawl Key, as in Huneeus et al. (2011) (Prospero et al., 2010). The free-running simulation results are compared with the measurements in Fig. 10, which appear to agree reasonably well. The differences between the two versions of our parameterization are small, likely because deposition fluxes are largely governed by transport and rainout processes, being the same in the two schemes. At Lake Barco, the model captures the seasonality and the magnitude of the deposited

ACPD
12, 13237–13298, 2012

dust, in contrast to some of the results in the AeroCom study (Huneeus et al., 2011). For the Tamiami Trail station a time shift of one month appears in the maximum deposition flux (the model maximum is in July, not in June as indicated by the measurements), and the model overestimates the bulk deposition flux. For the southernmost station, Little Crawl Key, the model captures the seasonality well though also overestimates the deposition maximum in summer, being the result of a too strong wet deposition flux. Since we are comparing different model and measurement periods, we cannot expect quantitative agreement, and we conclude that the model performs satisfactory for these locations.

5.2.3 Aerosol optical depth

The modelled AOD, which is dominated by dust at the selected stations, analysed at 550 nm wavelength, has been evaluated on a daily, monthly and annual basis. Although AERONET provides measurements of AOD at high temporal resolution of the order of minutes, the evaluation in this paper is based mainly on the daily and monthly averages, focussing on the seasonal dust cycle and not on specific dust events. Nevertheless, the daily averages provide a rather detailed view of the desert dust distribution. The monthly AOD is estimated from the daily values for each AERONET station, and the modelled AOD is calculated for the same days as those for which AERONET data is available. Whenever the MODIS (v5.1), MISR (v31) or MODIS Deep Blue (v.5.31) AOD is used, the monthly modelled values are calculated from all days of the month. For this evaluation the nudged simulations for DU1 and DU2 are used.

The comparison between daily measured and modelled AOD at the 19 AERONET stations for the year 2000 indicates reasonably good agreement for most stations. The linear correlation over all stations (Fig. 11) corroborates that the model reproduces many of the measured daily AODs. The biases are small for both versions of the emission scheme (−0.008 for DU1, and 0.014 for DU2) and the average and standard deviation are close to the measured values (Table 9). The overall performance is slightly better for the DU1_ERA40 simulation. In addition, we consider each station individually

ACPD
12, 13237–13298, 2012

and in groups according to the location (colours according to Fig. 3d). For the African stations (nos. 4, 6, 7, 9 and 16 in red), the model reproduces the daily AODs very well, e.g., in the outflow region of the dust (6: Cape Verde, 7: Dakar in Table 10). At the other three stations located in Central Africa, the model tends to underestimate the AOD. This can be attributed to a possible underestimation of both biomass burning and dust emissions in this area, the latter from the Bodélé Depression, for example, which is a major dust source region in N-Africa. In contrast to some other models, we have not tuned preferential dust sources such as the Bodélé Depression because we favour physical consistency within EMAC, with the risk of under-representing such pronounced source regions (Todd et al., 2008).

The daily AODs over the S-American and W-Atlantic stations (nos. 2, 5, 14 and 19) are represented well by the model with correlation coefficients in the range of 0.48 to 0.70 for DU1_ERA40 and 0.46 to 0.70 for DU2_ERA40 (Table 10). The model underestimates the AOD over the station Suriname (no. 19) in Northern S-America, and to a greater extent with the DU2_ERA40 simulation, possibly associated with the under-representation of anthropogenic aerosols in the model, notably biomass burning aerosols, which may influence this station. The model results for the stations in the Middle East (nos. 11, 15 and 17) correlate well with the daily AERONET AODs, though the model overestimates some peak values in April and May over Nes Ziona and Sede Boker in Israel. At the Arabian stations (nos. 3 and 18) the model performance is mediocre, for some months being better than others. During most of the time the model appears to overestimate the AOD. For the AOD over the Asian station (no. 1), located in S-Korea, we obtain a good linear correlation with the measurements, though the model underestimates AODs in January, March, November and December, while performing better in April, May, September and October (other months are absent from the observational dataset).

One station is located on an island in the Indian Ocean (no. 12, Maldives) where the model underestimates the AOD compared to the AERONET data in the period January to March, whereas the model performance is much better for the months of

ACPD
12, 13237–13298, 2012

New parameterization of dust emissions in EMAC

M. Astitha et al.

April to November (with the exception of July). This is likely related to pollution outflow from the Indian subcontinent during the dry season (Lawrence and Lelieveld, 2010), not represented in the model. Finally, for the stations located in S-Europe (nos. 8, 10 and 13; two in Italy and one in Spain) we obtain high correlations with the measurements for the Italian stations and a lower correlation with the Spanish data. The AODs over the Italian stations (Lampedusa and IMC Oristano) are typically overestimated by the model (both emission schemes, though better with DU1_ERA40), while in Southern Spain (El Arenosillo) the modelled AODs appear to be too low. Figure 11 summarizes these results into two global maps, showing the correlation coefficients for each of the AERONET stations, both for DU1_ERA40 and DU2_ERA40. This indicates that both versions of the emission scheme perform similarly in the Middle East, the Arabian Peninsula, S-Europe and some stations in S-America while DU1_ERA40 generally achieves the best agreement with AERONET data.

The monthly average AODs are calculated by only accounting for the days for which AERONET data are available, i.e., the same days from both the model results and the observations. Figure 12 shows the scatter plots for the two versions of our dust emission scheme. The upper panel shows the linear and the lower panel the logarithmic relationships, colour coded by the location of each station (Fig. 3d). It appears that the modelled monthly AOD correlates well with the AERONET observations for both schemes. The underestimation of the monthly AOD at the station Illorin (Nigeria) prevents a 1:1 regression. Again this may be related to the underrepresentation of anthropogenic aerosols in this location. Time series with the monthly AOD for all stations from the model results and from AERONET, MODIS-Terra and Deep Blue and/or MISR are included in the Supplement (Fig. S3), indicating generally good agreement.

By grouping the stations according to their location (Fig. 3d), the modelled monthly AODs agree well with the AERONET measurements for the S-American-Atlantic stations (purple), the Asian station in Anmyon (cyan, S-Korea), the Middle East (green) and the S- European stations (black). The comparison for the African stations (red) indicates good agreement, except for Illorin, as mentioned above. Poorer agreement

ACPD
12, 13237–13298, 2012

is obtained for the Arabian stations (blue) and the Indian Ocean station (black, Maldives). Similarly, generally good agreement is indicated by the annual AOD comparison (Fig. 13). It should be emphasized, however, that many of the AERONET measurement time series are incomplete, hence the "monthly" and "annual" data should be interpreted with care. Similar agreement with the AOD measurements is obtained for the two versions of our dust emission scheme for the African, Middle Eastern, S-European and S-American-Atlantic stations. Differences are more pronounced for the Arabian stations and Lampedusa (Italy), indicating better agreement using the DU1 scheme for Lampedusa and better agreement with DU2 for the Arabian stations.

The column aerosol mass burden ($\mu g\,cm^{-2}$) from the model and that derived from the MODIS-Terra satellite measurements is shown for the month of June 2000 in Fig. 14. We selected this month because of the generally intense dust activity in the large, arid areas such as N-Africa and the ensuing dust transport over the Atlantic Ocean. These plots only provide a qualitative evaluation, since this MODIS satellite data product is not validated to the same extent as the AOD. The outflow of desert dust towards the Atlantic Ocean appears to be well described using both emission schemes, matching both the spatial distribution pattern and the magnitude (Fig. 14). The column mass over the Indian Ocean and India is also in good agreement with the satellite-retrieved data, with DU2_ERA40 being closer to the observed column burden than DU1_ERA40. Unfortunately the N-African deserts are excluded from the MODIS data. Further, the DU2 scheme seems to overestimate the dust burden from the Asian deserts. Finally, the N-American arid areas are well represented by the DU1 scheme whereas DU2 again overestimates the dust load, while both schemes overestimate the amount of dust from S-America. Notwithstanding indications in the literature and from the MODIS data that S-America is only a weak dust source, especially compared to N-Africa (Prospero et al., 2002), both versions of the emission scheme generate significant dust plumes, while DU1 generates less dust and may be considered more representative. This is possibly related to the coarse resolution of the model, which smoothens the pronounced terrain, leading to too high friction velocities over the Patagonian desert. Again, this is

Discussion Paper | Discussion Paper | Discussion Paper | Discussion Paper |
ACPD
12, 13237–13298, 2012
New parameterization of dust emissions in EMAC
M. Astitha et al.

also a consequence of applying one consistent parameterization throughout the globe, whereas many models apply regionally tuned emission fluxes.

Nevertheless, the results from the AOD comparison indicate that both versions of our new dust emission parameterization adequately describe many of the sources, and that the EMAC model reproduces the dust transports over the Atlantic Ocean and the Mediterranean region realistically. The DU2 scheme, which includes an explicit soil particle size distribution, appears to perform better at locations like Anmyon, Dakar, Bahrain and Erdemli. Both schemes underestimate atmospheric dust at Illorin, possibly caused by too low emissions from the Bodélé Depression (Todd et al., 2008) and the under-representation of anthropogenic aerosols. Overall, the model simulations of the AOD in areas predominantly affected by airborne dust are comparable for both schemes, with DU1 performing slightly better than DU2. A recent study by Ridley et al. (2012) suggested that adding detail to the dust submicron size distribution in the AOD calculation (affecting only the dust optical properties and not the aerosol mass), leads to a reduction of the AOD over N-Africa, improving the agreement with observations. Also, Kok (2011) achieved a reduction in the overestimation of the clay fraction of the emitted dust aerosol by a theoretical expression of the particle size distribution, in contrast with the empirical expression. Both studies emphasize the emitted particle size distribution as a key factor in improving the representation of the global dust cycle. Though we did not assess the effects of changes in the emitted particle size distribution, we plan to address this issue in future work.

We emphasize that the criteria applied for the selection of dust-dominated AERONET stations do not preclude a role by anthropogenic aerosols. As discussed by Huneeus et al. (2011), data from stations with AODs (at 500–870 nm wavelength) between 0.4 and 1.2 may include a mixture of coarse and fine particles. Furthermore, the MODIS aerosol retrieval algorithm has difficulties when biomass burning and desert dust aerosols occur concurrently, typically overestimating the AOD (Kahn et al., 2009). Since anthropogenic aerosols are underrepresented in our simulations (we only account for sulphate), and also because the sea spray estimated by the model might not

ACPD
12, 13237–13298, 2012

be well represented over island stations, it may be expected that our model somewhat underestimates the AOD as compared to remote sensing observations.

6 Discussion and conclusion

The two versions of our dust emission scheme are primarily different in the explicit representation of soil particle size distributions. Whereas in DU1 the (tri-modal) soil particle size distribution is globally uniform, in DU2 it is explicitly accounted for based on the Zobler geographical soil texture classification and four soil populations, as listed in Table 3 (Tegen et al., 2002). This influences the threshold friction velocity, which triggers the dust mobilization and hence influences the emission fluxes. It should be stressed that the Zobler soil texture classification has been derived using wet sedimentation measurement techniques, which break the soil aggregates. This increases the number of free clay particles, thus underestimating the number of large size aggregates (Laurent et al., 2010; Kok, 2011). Furthermore, Laurent et al. (2006) mention that there is no direct relationship between the soil grain size distribution and the soil texture in the Northeast Asian deserts. An advanced technique, based on dry sedimentation, has been used by Chatenet et al. (1996), followed by Laurent et al. (2006, 2008, 2010) though the measurements are limited to several African, Arabian and Asian deserts and cannot be applied within a global framework at this stage. Nevertheless, making use of these data is planned as a next step in our work.

The model calculated atmospheric dust budgets based on the DU1 and DU2 dust emission schemes differ substantially (Table 5). In the free-running model the global source with DU2 is about 1000 $Tg\,yr^{-1}$ stronger than with DU1, and in the nudged simulations the difference is about 713 $Tg\,yr^{-1}$. It appears that the results of the nudged DU1_ERA40 simulation are closest to the median source of the AeroCom exercise, i.e., 1123 $Tg\,yr^{-1}$ (Huneeus et al., 2011). The DU2 scheme produces stronger emissions than DU1, mostly due to differences in the Asian and S-American deserts and to a lesser extent in N-Africa (Table 6). The stronger sources by DU2 primarily increase the

ACPD
12, 13237–13298, 2012

dust loads over the source regions, and it would be useful to have access to additional measurement data there. For the N-African deserts the total dust emissions by the two schemes do not deviate much except for DU2_ERA40, which seems relatively low (460 $\mathrm{Tg\,yr^{-1}}$). The two schemes also produce similar emissions in the Middle East and Australia. For S-Africa, Asia, N- and S-America, on the other hand, the differences can be a factor of two to three. This results from the substantially different soil particle size distributions.

The annual cycles by the DU1 and DU2 schemes are quite similar, also because the seasonality is predominantly determined by the meteorology rather than the soil classification (Fig. S2 in the Supplement shows the difference in the seasonal emissions between the two schemes). The differences are mostly regional and related to the threshold friction velocity (i.e., the particle size distribution, soil moisture, drag partition correction). Within Africa, the geographical patterns of DU1 and DU2 can differ also, the latter emitting less dust from the Sahara, Mauritania and the Bodélé Depression, and more in Libya and Algeria. This is a direct effect of the size distribution assigned to the soils in DU2, because in parts of the Sahara, the Bodélé Depression and Mauritania deserts typically have relatively coarse particles, while in Libya and Algeria more medium size particles are found (according to the Zobler classification).

Our evaluation of the concentrations, deposition fluxes and the AOD does not provide conclusive evidence about quality differences between our two schemes. Even though the explicit soil particle size distribution in DU2 is considered more realistic, the simpler DU1 scheme appears to perform better in several locations. The general conclusion from our evaluation is that DU1 performs slightly better in reproducing the remotely sensed AOD for the year 2000, especially in the vicinity of the sources, while DU2 leads to more realistic results in simulating the dust concentrations and deposition fluxes in remote locations. Future work, in which we aim to account for all classes of aerosols simultaneously and improve the representation of chemical "ageing" by dust particles in the atmosphere, will provide additional information to help evaluate our dust emission parameterization.

ACPD
12, 13237–13298, 2012

Supplementary material related to this article is available online at: http://www.atmos-chem-phys-discuss.net/12/13237/2012/ acpd-12-13237-2012-supplement.pdf.

Acknowledgements. The research leading to these results has received funding from the European Research Council under the European Union's Seventh Framework Programme (FP7/2007–2013)/ERC grant agreement no. 226144. The authors would like to thank J. Prospero for providing the dust concentration and deposition data, B. Herut for the data from Tel Shikmona (Haifa, Israel) and N. Huneeus for providing the datasets used in the AeroCom dust evaluation study. The authors would also like to thank P. Jöckel, H. Tost and A. Kerkweg for the helpful discussions during the coding in the EMAC model. We thank the Principle Investigators and their staff for establishing and maintaining the AERONET sites used in this investigation. Analyses used in this paper were produced with the Giovanni online data system, developed and maintained by the NASA GES DISC. We acknowledge the mission scientists and Principal Investigators who provided the data used in this research effort (MODIS Terra, MISR, Deep Blue).

References

Alfaro, S. C. and Gomes L.: Modeling mineral aerosol production by wind erosion: emission intensities and aerosol size distributions in source areas, J. Geophys. Res., 106, 18075–18084, 2001.

Arimoto, R., Duce, R. A., Ray, B. J., Ellis, W. G., Cullen, J. D., and Merrill, J. T.: Trace-elements in the atmosphere over the North-Atlantic, J. Geophys. Res.-Atmos., 100, 1199–1213, 1995.

Astitha, M., Kallos, G., Spyrou, C., O'Hirok, W., Lelieveld, J., and Denier van der Gon, H. A. C.: Modelling the chemically aged and mixed aerosols over the eastern central Atlantic Ocean – potential impacts, Atmos. Chem. Phys., 10, 5797–5822, doi:10.5194/acp-10-5797-2010, 2010.

Balkanski, Y., Schulz, M., Claquin, T., Moulin, C., and Ginoux, P.: Global emissions of mineral aerosol: formulation and validation using satellite imagery, in: Emission of Atmospheric Trace

Discussion Paper | Discussion Paper | Discussion Paper | Discussion Paper |

ACPD

12, 13237–13298, 2012

New parameterization of dust emissions in EMAC

M. Astitha et al.

Compounds, edited by: Granier, C., Artaxo, P., and Reeves, C. E., Kluwer, Amsterdam, The Netherlands, 239–267, 2004.
Callot, Y., Marticorena, B., and Bergametti, G.: Geomorphologic approach for modelling the surface features of arid environments in a model of dust emissions: application to the Sahara desert, Geodin. Acta, 13, 245–270, doi:10.1016/S0985-3111(00)01044-5, 2000.
Chatenet, B., Marticorena, B., Gomes, L., and Bergametti, G.: Assessing the microped size distributions of desert soils erodible by wind, Sedimentology, 43, 901–911, doi:10.1111/j.1365-30 3091.1996.tb01509.x, 1996.
Cheng, T., Peng, Y., Feichter, J., and Tegen, I.: An improvement on the dust emission scheme in the global aerosol-climate model ECHAM5-HAM, Atmos. Chem. Phys., 8, 1105–1117, doi:10.5194/acp-8-1105-2008, 2008.
D'Almeida, G. A.: On the variability of desert aerosol radiative characteristics, J. Geophys. Res., 92, 3017–3026, 1987.
Darmenova, K., Sokolik, I. N., Shao, Y., Marticorena, B., and Bergametti G.: Development of a physically based dust emission module within the Weather Research and Forecasting (WRF) model: assessment of dust emission parameterizations and input parameters for source regions in Central and East Asia, J. Geophys. Res., 114, D14201, doi:10.1029/2008JD011236, 2009.
De Meij, A. and Lelieveld, J.: Evaluating aerosol optical properties observed by ground-based and satellite remote sensing over the Mediterranean and the Middle East in 2006, Atmos. Res., 99, 415–433, 2011.
Forster, P., Ramaswamy, V., Artaxo, P., Berntsen, T., Betts, R., Fahey, D. W., Haywood, J., Lean, J., Lowe, D. C., Myhre, G., Nganga, J., Prinn, R., Raga, G., Schulz, M., and Van Dorland, R.: Changes in atmospheric constituents and in radiative forcing, in: Climate Change 2007: The Physical Science Basis, Contribution of Working Group I to the Fourth Assessment Report of the Intergovernmental Panel on Climate Change, edited by: Solomon, S., Qin, D., Manning, M., Chen, Z., Marquis, M., Averyt, K. B., Tignor, M., and Miller, H. L., Cambridge University Press, Cambridge, UK and New York, NY, USA, 2007.
Ginoux, P., Chin, M., Tegen, I., Prospero, J. M., Holben, B., Dubovik, O., and Lin, S.: Sources and distributions of dust aerosols simulated with the GOCART model, J. Geophys. Res., 106, 20255–20274, doi:10.1029/2000JD000053, 2001.

ACPD
12, 13237–13298, 2012

Gläser, G., Kerkweg, A., and Wernli, H.: The Mineral Dust Cycle in EMAC 2.40: sensitivity to the spectral resolution and the dust emission scheme, Atmos. Chem. Phys., 12, 1611–1627, doi:10.5194/acp-12-1611-2012, 2012.
Grini, A., Zender, C. S., and Colarco, P.: Saltation sandblasting behaviour during mineral dust aerosol production, Geophys. Res. Lett., 29, 1868, doi:10.1029/2002GL015248, 2002.
Hillel, D.: Fundamentals of Soil Physics, Academic Press, New York, 1980.
Huneeus, N., Schulz, M., Balkanski, Y., Griesfeller, J., Prospero, J., Kinne, S., Bauer, S., Boucher, O., Chin, M., Dentener, F., Diehl, T., Easter, R., Fillmore, D., Ghan, S., Ginoux, P., Grini, A., Horowitz, L., Koch, D., Krol, M. C., Landing, W., Liu, X., Mahowald, N., Miller, R., Morcrette, J.-J., Myhre, G., Penner, J., Perlwitz, J., Stier, P., Takemura, T., and Zender, C. S.: Global dust model intercomparison in AeroCom phase I, Atmos. Chem. Phys., 11, 7781–7816, doi:10.5194/acp-11-7781-2011, 2011.
Iversen, J. D. and White, B. R.: Saltation threshold on Earth, Mars, and Venus, Sedimentology, 29, 111–119, 1982.
Jöckel, P., Sander, R., Kerkweg, A., Tost, H., and Lelieveld, J.: Technical Note: The Modular Earth Submodel System (MESSy) – a new approach towards Earth System Modeling, Atmos. Chem. Phys., 5, 433–444, doi:10.5194/acp-5-433-2005, 2005.
Jöckel, P., Tost, H., Pozzer, A., Brühl, C., Buchholz, J., Ganzeveld, L., Hoor, P., Kerkweg, A., Lawrence, M. G., Sander, R., Steil, B., Stiller, G., Tanarhte, M., Taraborrelli, D., van Aardenne, J., and Lelieveld, J.: The atmospheric chemistry general circulation model ECHAM5/MESSy1: consistent simulation of ozone from the surface to the mesosphere, Atmos. Chem. Phys., 6, 5067–5104, doi:10.5194/acp-6-5067-2006, 2006.
Jöckel, P., Kerkweg, A., Pozzer, A., Sander, R., Tost, H., Riede, H., Baumgaertner, A., Gromov, S., and Kern, B.: Development cycle 2 of the Modular Earth Submodel System (MESSy2), Geosci. Model Dev., 3, 717–752, doi:10.5194/gmd-3-717-2010, 2010.
Kahn, R. A., Nelson, D. L., Garay, M., Levy, R. C., Bull, M. A., Diner, D. J., Martonchik, J. V., Paradise, S. R., Hansen, E. G., and Remer, L. A.: MISR Aerosol product attributes, and statistical comparisons with MODIS, IEEE T. Geosci. Remote, 47, 4095–4114, 2009.
Kallos, G., Astitha, M., Katsafados, P., and Spyrou, C.: Long-range transport of anthropogenically and naturally produced particulate matter in the Mediterranean and North Atlantic – current state of knowledge, J. Appl. Meteor. Clim., 46, 1230–1251, 2007.
Kerkweg, A., Buchholz, J., Ganzeveld, L., Pozzer, A., Tost, H., and Jöckel, P.: Technical Note: An implementation of the dry removal processes DRY DEPosition and SEDImenta-

tion in the Modular Earth Submodel System (MESSy), Atmos. Chem. Phys., 6, 4617–4632, doi:10.5194/acp-6-4617-2006, 2006a.
Kerkweg, A., Sander, R., Tost, H., and Jöckel, P.: Technical note: Implementation of prescribed (OFFLEM), calculated (ONLEM), and pseudo-emissions (TNUDGE) of chemical species in the Modular Earth Submodel System (MESSy), Atmos. Chem. Phys., 6, 3603–3609, doi:10.5194/acp-6-3603-2006, 2006b.
Kok, J. F.: A scaling theory for the size distribution of emitted dust aerosols suggest climate models underestimate the size of the global dust cycle, Proc. Natl. Acad. Sci., 108, 1016–1021, 2011.
Landgraf, J. and Crutzen, P. J.: An efficient method for online calculations of photolysis and heating rates, J. Atmos. Sci., 55, 863–878, 1998.
Lauer, A., Eyring, V., Hendricks, J., Jöckel, P., and Lohmann, U.: Global model simulations of the impact of ocean-going ships on aerosols, clouds, and the radiation budget, Atmos. Chem. Phys., 7, 5061–5079, doi:10.5194/acp-7-5061-2007, 2007.
Laurent, B., Marticorena, B., Bergametti, G., Chazette, P., Maignan, F., and Schmechtig, C.: Simulation of the mineral dust emission frequencies from desert areas of China and Mongolia using an aerodynamic roughness length map derived from the POLDER/ADEOS-1 surface products, J. Geophys. Res., 110, D18S04, doi:10.1029/2004JD005013, 2005.
Laurent, B., Marticorena, B., Bergametti, G., and Mei, F.: Modeling mineral dust emissions from Chinese and Mongolian deserts, Global Planet. Change, 52, 121–141, 2006.
Laurent, B., Marticorena, B., Bergametti, G., Leon, J.-F., and Mahowald, N.: Modeling mineral dust emissions from the Sahara desert using new surface properties and soil database, J. Geophys. Res., 113, D14218, doi:10.1029/2007JD009484, 2008.
Laurent, B., Tegen, I., Heinold, B., Schepanski, K., Weinzierl, B. and Esselborn, M.: A model study of Saharan dust emissions and distributions during the SAMUM-1 campaign, J. Geophys. Res., 115, D21210, doi:10.1029/2009JD012995, 2010.
Lawrence, M. G. and Lelieveld, J.: Atmospheric pollutant outflow from southern Asia: a review, Atmos. Chem. Phys., 10, 11017–11096, doi:10.5194/acp-10-11017-2010, 2010.
Lelieveld, J., Brühl, C., Jöckel, P., Steil, B., Crutzen, P. J., Fischer, H., Giorgetta, M. A., Hoor, P., Lawrence, M. G., Sausen, R., and Tost, H.: Stratospheric dryness: model simulations and satellite observations, Atmos. Chem. Phys., 7, 1313–1332, doi:10.5194/acp-7-1313-2007, 2007.

Mahowald, N. M., Baker, A. R., Bergametti, G., Brooks, N., Duce, R. A., Jickells, T. D., Kubilay, N., Prospero, J. N., and Tegen, I.: Atmospheric global dust cycle and and iron inputs to the ocean, Global Biogeochem. Cy., 19, GB4025, doi:10.1029/2004GB002402, 2005.
Marticorena, B. and Bergametti, G.: Modeling the atmospheric dust cycle: 1. Design of a soil-derived dust emission scheme, J. Geophys. Res., 100, 16415–16430, 1995.
Marticorena, B., Bergametti, G., Aumont, B., Callot, Y., N'Doume', C., and Legrand, M.: Modeling the atmospheric dust cycle: 2. Simulation of Saharan dust sources, J. Geophys. Res., 102, 4387–4404, 1997.
Nickovic, S., Kallos, G., Papadopoulos, A., and Kakaliagou, O.: A model for prediction of desert dust cycle in the atmosphere, J. Geophys. Res., 106, 18113–18130, doi:10.1029/2000JD900794, 2001.
Olson, J.: World ecosystems (WE1.4): digital raster data on a 10 minute geographic 1080 (2160 grid square), Global Ecosystem Database, Version 1.0: DISC A, edited by: NOAA National Geophysical Data Center, Boulder, CO, 1992.
Pérez, C., Nickovic, S., Baldasano, J. M., Sicard, M., Rocadenbosch, F., and Cachorro, V. E.: A long Saharan dust event over the Western Mediterranean: Lidar, Sun photometer observations, and regional dust modeling, J. Geophys. Res., 111, D15214, doi:10.1029/2005JD006579, 2006.
Pérez, C., Haustein, K., Janjic, Z., Jorba, O., Huneeus, N., Baldasano, J. M., Black, T., Basart, S., Nickovic, S., Miller, R. L., Perlwitz, J. P., Schulz, M., and Thomson, M.: Atmospheric dust modeling from meso to global scales with the online NMMB/BSC-Dust model – Part 1: Model description, annual simulations and evaluation, Atmos. Chem. Phys., 11, 13001–13027, doi:10.5194/acp-11-13001-2011, 2011.
Pozzer, A., de Meij, A., Pringle, K. J., Tost, H., Doering, U. M., van Aardenne, J., and Lelieveld, J.: Distributions and regional budgets of aerosols and their precursors simulated with the EMAC chemistry-climate model, Atmos. Chem. Phys., 12, 961–987, doi:10.5194/acp-12-961-2012, 2012.
Pringle, K. J., Tost, H., Message, S., Steil, B., Giannadaki, D., Nenes, A., Fountoukis, C., Stier, P., Vignati, E., and Lelieveld, J.: Description and evaluation of GMXe: a new aerosol submodel for global simulations (v1), Geosci. Model Dev., 3, 391–412, doi:10.5194/gmd-3-391-2010, 2010.

ACPD
12, 13237–13298, 2012

New parameterization of dust emissions in EMAC

M. Astitha et al.

Prospero, J. M.: The atmospheric transport of particles to the ocean, in: Particle Flux in the Ocean, edited by: Ittekkot, V., Schäfer, P., Honjo, S., and Depetris, P. J., John Wiley and Sons Ltd., New York, 1996.

Prospero, J. M.: Long-term measurements of the transport of African mineral dust to the Southeastern United States: implications for regional air quality, J. Geophys. Res.-Atmos., 104, 15917–15927, 1999.

Prospero, J. M., Uematsu, M., and Savoie, D. L.: Mineral Aerosol Transport to the Pacific Ocean, edited by: Riley, J. P., Academic Press, New York, 187–218, 1989.

Prospero, J. M., Ginoux, P., Torres, O., Nicholson, S. E., and Gill, T. E.: Environmental characterization of global sources of atmospheric soil dust identified with the nimbus 7 total ozone mapping spectrometer (TOMS) absorbing aerosol product, Rev. Geophys., 40, 1002, doi:10.1029/2000RG000095, 2002.

Prospero, J. M., Landing, W. M., and Schulz, M.: African dust deposition to Florida: temporal and spatial variability and comparisons to models, J. Geophys. Res., 115, D13304, doi:10.1029/2009JD012773, 2010.

Ramanathan, V., Crutzen, P. J., Kiehl, J. T., Rosenfeld, D.: Aerosols, climate and the hydrological cycle, Science, 294, 2119, doi:10.1126/science.1064034, 2001.

Ridley, D. A., Heald, C. L., and Ford, B.: North African dust transport and deposition: a satellite and model perspective, J. Geophys. Res., 117, D02202, doi:10.1029/2011JD016794, 2012.

Roeckner, E., Brokopf, R., Esch, M., Giorgetta, M., Hagemann, S., Kornblueh, L., Manzini, E., Schlese, U., and Schulzweida, U.: Sensitivity of simulated climate to horizontal and vertical resolution in the ECHAM5 atmosphere model, J. Climate, 19, 3371–3791, doi:10.1175/JCLI3824.1, 2006.

Schenk, H. J. and Jackson, R. B.: ISLSCP II ecosystem rooting depths, in: ISLSCP Initiative II Collection, Data set, edited by: Hall Forrest, G., Collatz, G., Meeson, B., Los, S., Brown de Colstoun, E., and Landis, D., available online: http://daac.ornl.gov/ from Oak Ridge National Laboratory Distributed Active Archive Center, Oak Ridge, Tennessee,USA, doi:10.3334/ORNLDAAC/929, 2009.

Scholes, R. J. and Brown de Colstoun, E.: ISLSCP II Global Gridded Soil Characteristics, in: ISLSCP Initiative II Collection, Data set, edited by: Hall Forrest, G., Collatz, G., Meeson, B., Los, S., Brown de Colstoun, E., and Landis, D., available online: http://daac.ornl.gov/ from Oak Ridge National Laboratory Distributed Active Archive Center, Oak Ridge, Tennessee, USA, doi:10.3334/ORNLDAAC/1004, 2011.

ACPD
12, 13237–13298, 2012

New parameterization of dust emissions in EMAC

M. Astitha et al.

Schulz, M., Balkanski Y. J., Guelle W., and Dulac F.: Role of aerosol sizedistribution and source location in a three-dimensional simulation of a Saharan dust episode tested against satellite-derived optical thickness, J. Geophys. Res., 103, 10579–10592, 1998.
Shao, Y.: Simplification of a dust emission scheme and comparison with data, J. Geophys. Res., 109, D10202, doi:10.1029/2003JD004372, 2004.
Shao, Y., Raupach, M. R., and Findlater, P. A.: The effect of saltation bombardment on the entrainment of dust by wind, J. Geophys. Res., 98, 12719–12726, doi:10.1029/93JD00396, 1993.
Shao, Y., Ishizuka, M., Mikami, M., and Leys, J. F.: Parameterization of size-resolved dust emission and validation with measurements, J. Geophys. Res., 116, D08203, doi:10.1029/2010JD014527, 2011.
Sokolik, I. N. and Toon, O. B.: Direct radiative forcing by anthropogenic airborne mineral aerosols, Nature, 381, 681–683, 1996.
Spyrou, C., Mitsakou, C., Kallos, G., Louka, P., and Vlastou, G.: An improved limited area model for describing the dust cycle in the atmosphere, J. Geophys. Res., 115, D17211, doi:10.1029/2009JD013682, 2010.
Stier, P., Feichter, J., Kinne, S., Kloster, S., Vignati, E., Wilson, J., Ganzeveld, L., Tegen, I., Werner, M., Balkanski, Y., Schulz, M., Boucher, O., Minikin, A., and Petzold, A.: The aerosol-climate model ECHAM5-HAM, Atmos. Chem. Phys., 5, 1125–1156, doi:10.5194/acp-5-1125-2005, 2005.
Tegen, I. and Lacis, A. A.: Modeling of particle size distribution and its influence on the radiative properties of mineral dust aerosol, J. Geophys. Res., 101, 19237–19244, 1996.
Tegen, I., Harrison, S. P., Kohfeld, K., Prentice, I. C., Coe, M., and Heimann, M.: Impact of vegetation and preferential source areas on global dust aerosol: results from a model study, J. Geophys. Res.-Atmos., 107, 4576, doi:10.1029/2001JD000963, 2002.
Textor, C., Schulz, M., Guibert, S., Kinne, S., Balkanski, Y., Bauer, S., Berntsen, T., Berglen, T., Boucher, O., Chin, M., Dentener, F., Diehl, T., Easter, R., Feichter, H., Fillmore, D., Ghan, S., Ginoux, P., Gong, S., Grini, A., Hendricks, J., Horowitz, L., Huang, P., Isaksen, I., Iversen, I., Kloster, S., Koch, D., Kirkevåg, A., Kristjansson, J. E., Krol, M., Lauer, A., Lamarque, J. F., Liu, X., Montanaro, V., Myhre, G., Penner, J., Pitari, G., Reddy, S., Seland, Ø., Stier, P., Takemura, T., and Tie, X.: Analysis and quantification of the diversities of aerosol life cycles within AeroCom, Atmos. Chem. Phys., 6, 1777–1813, doi:10.5194/acp-6-1777-2006, 2006.

ACPD
12, 13237–13298, 2012

Textor, C., Schulz, M., Guibert, S., Kinne, S., Balkanski, Y., Bauer, S., Berntsen, T., Berglen, T., Boucher, O., Chin, M., Dentener, F., Diehl, T., Feichter, J., Fillmore, D., Ginoux, P., Gong, S., Grini, A., Hendricks, J., Horowitz, L., Huang, P., Isaksen, I. S. A., Iversen, T., Kloster, S., Koch, D., Kirkevåg, A., Kristjansson, J. E., Krol, M., Lauer, A., Lamarque, J. F., Liu, X., Montanaro, V., Myhre, G., Penner, J. E., Pitari, G., Reddy, M. S., Seland, Ø., Stier, P., Takemura, T., and Tie, X.: The effect of harmonized emissions on aerosol properties in global models – an AeroCom experiment, Atmos. Chem. Phys., 7, 4489–4501, doi:10.5194/acp-7-4489-2007, 2007.

Timmreck, C. and Schulz, M.: Significant dust simulation differences in nudged and climatological operation mode of the AGCM ECHAM, J. Geophys. Res., 109, D13202, doi:10.1029/2003JD004381, 2004.

Todd, M. C., Bou Karam, D., Cavazos, C., Bouet, C., Heinold, B., Baldasano, J. M., Cautenet, G., Koren, I., Perez, C., Solmon, F., Tegen, I., Tulet, P., Washington, R., Zakey, A.: Quantifying uncertainty in estimates of mineral dust flux: an intercomparison of model performance over the Bodélé Depression, Northern Chad, J. Geophys. Res., 113, D24107, doi:10.1029/2008JD010476, 2008.

Tost, H., Jöckel, P., Kerkweg, A., Sander, R., and Lelieveld, J.: Technical note: A new comprehensive SCAVenging submodel for global atmospheric chemistry modelling, Atmos. Chem. Phys., 6, 565–574, doi:10.5194/acp-6-565-2006, 2006a.

Tost, H., Jöckel, P., and Lelieveld, J.: Influence of different convection parameterisations in a GCM, Atmos. Chem. Phys., 6, 5475–5493, doi:10.5194/acp-6-5475-2006, 2006b.

Tost, H., Jöckel, P., and Lelieveld, J.: Lightning and convection parameterisations – uncertainties in global modelling, Atmos. Chem. Phys., 7, 4553–4568, doi:10.5194/acp-7-4553-2007, 2007.

Tost, H., Lawrence, M. G., Brühl, C., Jöckel, P., The GABRIEL Team, and The SCOUT-O3-DARWIN/ACTIVE Team: Uncertainties in atmospheric chemistry modelling due to convection parameterisations and subsequent scavenging, Atmos. Chem. Phys., 10, 1931–1951, doi:10.5194/acp-10-1931-2010, 2010.

Vignati, E., Wilson, J., and Stier, P.: M7: an efficient size-resolved aerosol microphysics module for large-scale aerosol transport models, J. Geophys. Res., 109, D22202, doi:10.1029/2003JD004485, 2004.

ACPD
12, 13237–13298, 2012

Zender, C. S., Bian, H., and Newman, D.: Mineral Dust Entrainment and Deposition (DEAD) model: description and 1990s dust climatology, J. Geophys. Res., 108, 4416, doi:10.1029/2002JD002775, 2003.

ACPD
12, 13237–13298, 2012

New parameterization of dust emissions in EMAC

M. Astitha et al.

Table 1. EMAC sub-models used in this study.

Submodel	Description	Reference
M7	Aerosol microphysics	Vignati et al. (2004)
DRYDEP	Dry deposition	Kerkweg et al. (2006a)
SCAV	Wet deposition	Tost et al. (2006a)
SEDI	Sedimentation of aerosol particles	Kerkweg et al. (2006a)
MECCA1	Atmospheric chemistry	Sander et al. (2005)
OFFEMIS	Prescribed emissions of trace gases and aerosols	Kerkweg et al. (2006b)
ONEMIS	On-line calculated emissions of trace gases and aerosols	Kerkweg et al. (2006b)
RAD4ALL	ECHAM5 radiation scheme as MESSy submodel	Roeckner et al. (2006); Jöckel et al. (2006)
JVAL	photolysis rates	based on Landgraf and Crutzen (1998)
AEROPT	Aerosol Optical Depth	Lauer et al. (2007), Pozzer et al. (2012)
CLOUD	ECHAM5 cloud scheme as MESSy submodel	Roeckner et al. (2006, and references therein)
CONVECT	convection parameterizations	Tost et al. (2010)
CVTRANS	convective tracer transport	Tost et al. (2006b)
LNOX	lightning NO_x production	Tost et al. (2007)
TNUDGE	Newtonian relaxation of species as pseudo-emissions	Kerkweg et al. (2006b)
TROPOP	Tropopause and other diagnostics	Jöckel et al. (2006)

ACPD
12, 13237–13298, 2012

Table 2. Olson ecosystem biomes selected for the dust emission scheme.

No.	Biomes
1	Desert, mostly bare stone, clay, sand
2	Sand desert, partly blowing dunes
3	Semidesert/desert shrub/sparse grass
4	Cool/cold shrub semidesert/steppe
5	Salt/soda flat desert playas, occasionally with intermittent lakes

ACPD
12, 13237–13298, 2012

Table 3. Zobler soil texture classification and mass fraction for each soil size population after Tegen et al. (2002). For all particle sizes the geometric standard deviation σ_g is 2.0.

Soil Type	mf_1 (D_{v1} = 707 µm)	mf_2 (D_{v2} = 158 µm)	mf_3 (D_{v3} = 15 µm)	mf_4 (D_{v4} = 2 µm)
Coarse	0.43	0.40	0.17	0
Medium	0	0.37	0.33	0.30
Fine	0	0	0.33	0.67
Coarse-medium	0.10	0.50	0.20	0.20
Coarse-fine	0	0.50	0.12	0.38
Medium-fine	0	0.27	0.25	0.48
Coarse-medium-fine	0.23	0.23	0.19	0.35

ACPD
12, 13237–13298, 2012

Table 4. Characteristics of the two versions of the dust emission scheme.

Input parameters and calculated fields	DU1	DU2
Olson world ecosystem biomes	Yes	Yes
Clay fraction of the soil	Yes	Yes
Rooting Depth	Yes	Yes
Vegetation area index	Yes	Yes
Meteorological fields (temperature, pressure, humidity, soil moisture, friction velocity)	Yes	Yes
Threshold friction velocity over smooth surfaces	u_{*ts} (for $D_p = 60\,\mu m$)	$u_{*ts}(D_p)$
Drag partition correction (fixed z_o,z_{os})	Yes	Yes
Soil moisture correction	Yes	Yes
Zobler soil texture classification	No	Yes
Source Size Distribution	Globally uniform tri-modal distribution (D'Almeida, 1987)	Explicit assignment of particle size in each grid cell (Table 3)
Transport size distribution	8-size bin distribution after Perez et al. (2006)	As in DU1
Horizontal Flux	H	$H(D_p)$
Vertical Flux	$V_j = F_1 B \alpha H \sum_{i=1}^{3} m_i M_{i,j}$	$V_j = F_2 B \alpha H_{tot} \sum_{i=1}^{4} \mathrm{mf}_i M_{ij}$
Sandblasting efficiency (α)	$a = 10^{0.134(\%\ \mathrm{clay})-6}$ clay < 20% $a = 1.0 \times 10^{-6}$ 20% ≤ clay < 45% $a = 1.0 \times 10^{-7}$ clay ≥ 45%	As in DU1

ACPD
12, 13237–13298, 2012

New parameterization of dust emissions in EMAC

M. Astitha et al.

Title Page
Abstract | Introduction
Conclusions | References
Tables | Figures
◀◀ | ▶▶
◀ | ▶
Back | Close
Full Screen / Esc
Printer-friendly Version
Interactive Discussion

Table 5. Atmospheric dust budgets by the different emissions schemes, compared with the AeroCom median values as presented in Huneeus et al. (2011).

	Emissions ($Tg yr^{-1}$)	Load (Tg)	Dry ($Tg yr^{-1}$)	Sedi ($Tg yr^{-1}$)	Wet ($Tg yr^{-1}$)	Lifetime (days) (load/deposition)
AeroCom Median	1123	15.8	396	314	357	4.6
DU1	1841	23.2	82	573	1161	4.7
DU2	2860	32.2	138	841	1846	4.2
DU1_ERA40	1472	19.9	67	484	904	4.9
DU2_ERA40	2185	26.1	104	675	1392	4.4

ACPD
12, 13237–13298, 2012

Table 6. Regional dust emissions ($Tg\,yr^{-1}$) (regions shown in Fig. 3c) for the different simulations.

	N. Africa ($Tg\,yr^{-1}$)	S. Africa ($Tg\,yr^{-1}$)	Middle East ($Tg\,yr^{-1}$)	Asia ($Tg\,yr^{-1}$)	N. America ($Tg\,yr^{-1}$)	S. America ($Tg\,yr^{-1}$)	Australia ($Tg\,yr^{-1}$)
AeroCom Median	792	11.8	128	137	2	9.8	30.7
DU1	659	57.4	244	395	30	367	34.7
DU2	611	99.4	325	934	65	681	47.8
DU1_ERA40	528	54.1	182	283	22	314	35.7
DU2_ERA40	460	93.2	233	639	48	569	49.7

ACPD
12, 13237–13298, 2012

Table 7. Statistics of the annual average dust concentrations. January has been excluded.

	Average ($\mu g\, m^{-3}$)	Linear regression	Correlation coefficient	Bias ($\mu g\, m^{-3}$)	RMSE ($\mu g\, m^{-3}$)
Observations	4.40 ± 7.63				
DU1	5.24 ± 14.28	$y = 1.60x - 1.81$	0.86	0.84	8.56
DU2	6.33 ± 14.00	$y = 1.54x - 0.46$	0.84	1.93	8.67
DU1_ERA40	4.47 ± 11.03	$y = 1.27x - 1.11$	0.88	0.07	5.56
DU2_ERA40	5.10 ± 10.02	$y = 1.14x + 0.08$	0.87	0.69	5.03

Discussion Paper | Discussion Paper | Discussion Paper | Discussion Paper |

ACPD
12, 13237–13298, 2012

New parameterization of dust emissions in EMAC

M. Astitha et al.

ACPD
12, 13237–13298, 2012

New parameterization of dust emissions in EMAC

M. Astitha et al.

Table 8. Statistics of the monthly average dust concentrations. January has been excluded.

	Average ($\mu g\,m^{-3}$)	Linear regression	Correlation coefficient	Bias ($\mu g\,m^{-3}$)	RMSE ($\mu g\,m^{-3}$)
Observations	4.47 ± 9.16				
DU1	5.03 ± 24.31	$y = 0.82x + 1.37$	0.31	0.55	23.15
DU2	5.90 ± 22.71	$y = 0.85x + 2.08$	0.34	1.42	21.37
DU1_ERA40	4.29 ± 23.05	$y = 1.29x - 1.51$	0.52	−0.18	19.89
DU2_ERA40	4.74 ± 20.80	$y = 1.23x - 0.77$	0.54	0.26	17.56

Table 9. Statistics of the daily average AOD for 19 AERONET stations.

	Average ($\mu g\, m^{-3}$)	Linear regression	Correlation coefficient	Bias ($\mu g\, m^{-3}$)	RMSE ($\mu g\, m^{-3}$)
Observations	0.298 ± 0.28				
DU1_ERA40	0.29 ± 0.28	$y = 0.57x + 0.12$	0.55	−0.008	0.27
DU2_ERA40	0.31 ± 0.33	$y = 0.54x + 0.15$	0.46	0.014	0.33

ACPD
12, 13237–13298, 2012

New parameterization of dust emissions in EMAC

M. Astitha et al.

Table 10. Statistics of the 19 AERONET stations (daily average AOD). The station numbers correspond to the locations shown in Fig. 3d.

Stations (#)	Station Name	DU1_ERA40	DU2_ERA40
1	Anmyon	$y = 0.55x - 0.03$, $r = 0.55$	$y = 0.73x - 0.03$, $r = 0.44$
2	Arica	$y = 0.69x + 0.006$, $r = 0.49$	$y = 1.26x - 0.003$, $r = 0.48$
3	Bahrain	$y = 0.31x + 0.27$, $r = 0.36$	$y = 0.54x + 0.34$, $r = 0.39$
4	Banizoumbou	$y = 0.26x + 0.33$, $r = 0.36$	$y = 0.19x + 0.26$, $r = 0.32$
5	Barbados	$y = 0.76x + 0.04$, $r = 0.51$	$y = 0.74x + 0.05$, $r = 0.53$
6	Capo_Verde	$y = 0.88x + 0.23$, $r = 0.66$	$y = 0.81x + 0.19$, $r = 0.64$
7	Dakar	$y = 1.41x + 0.13$, $r = 0.70$	$y = 1.29x + 0.10$, $r = 0.69$
8	El_Arenosillo	$y = 0.44x + 0.05$, $r = 0.38$	$y = 0.48x + 0.06$, $r = 0.35$
9	Illorin	$y = 0.21x + 0.35$, $r = 0.55$	$y = 0.17x + 0.26$, $r = 0.56$
10	IMC_Oristano	$y = 1.69x - 0.08$, $r = 0.82$	$y = 1.95x - 0.10$, $r = 0.80$
11	IMS-METU-ERD	$y = 0.51x + 0.01$, $r = 0.61$	$y = 0.56x - 0.009$, $r = 0.60$
12	Kaashidhoo	$y = 0.50x + 0.005$, $r = 0.59$	$y = 0.52x + 0.02$, $r = 0.52$
13	Lampedusa	$y = 2.21x - 0.04$, $r = 0.84$	$y = 2.66x - 0.08$, $r = 0.84$
14	La_Parguera	$y = 1.15x - 0.02$, $r = 0.70$	$y = 1.06x - 0.02$, $r = 0.70$
15	Nes_Ziona	$y = 1.01x - 0.02$, $r = 0.62$	$y = 1.27x - 0.05$, $r = 0.63$
16	Ouagadougou	$y = 0.24x + 0.27$, $r = 0.42$	$y = 0.21x + 0.22$, $r = 0.41$
17	SEDE_BOKER	$y = 1.17x + 0.04$, $r = 0.66$	$y = 1.45x + 0.03$, $r = 0.69$
18	Solar_Village	$y = 0.39x + 0.46$, $r = 0.36$	$y = 0.60x + 0.63$, $r = 0.37$
19	Surinam	$y = 0.53x + 0.016$, $r = 0.48$	$y = 0.45x + 0.02$, $r = 0.46$

ACPD
12, 13237–13298, 2012

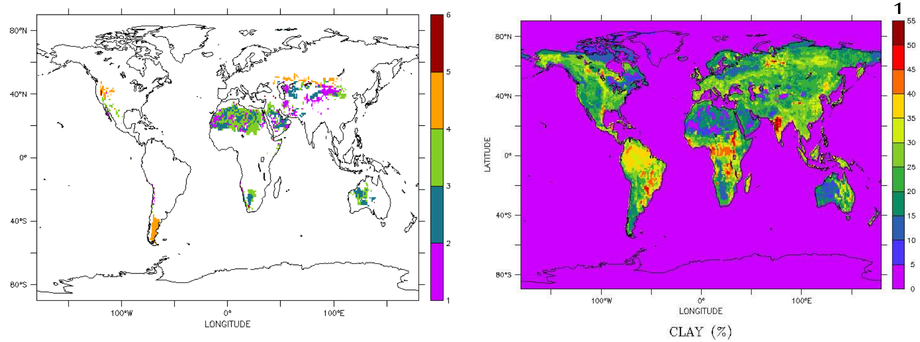

Fig. 1. Left plot: Olson global ecosystem biomes. The indices on the colour bar correspond to the values in Table 2. Right plot: Clay content of the soil (%). Both plots at 1°×1° resolution.

ACPD
12, 13237–13298, 2012

New parameterization of dust emissions in EMAC

M. Astitha et al.

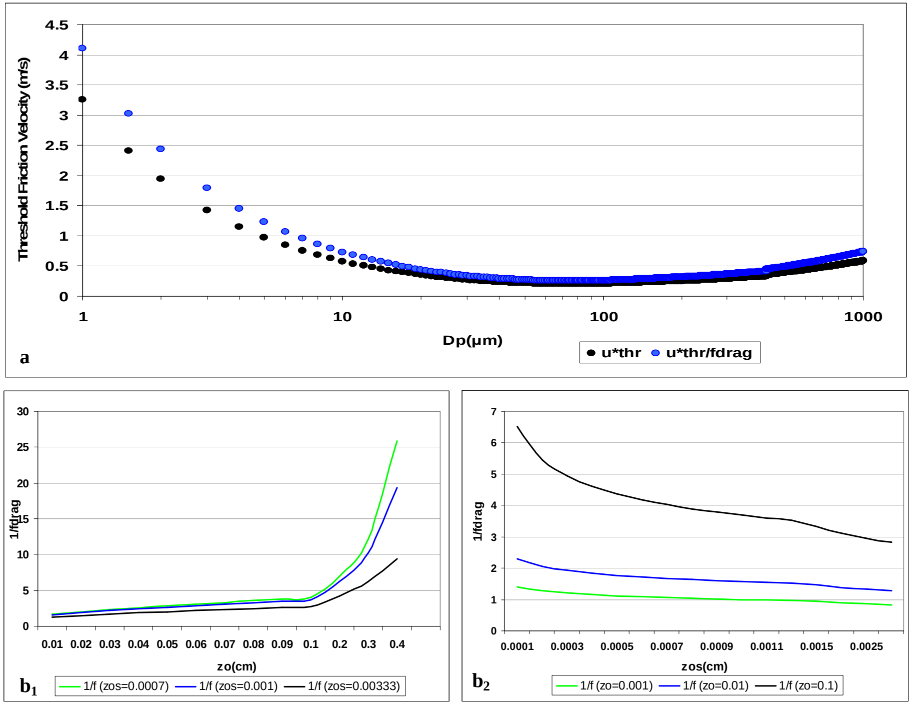

Fig. 2. (a) Dependence of the threshold friction velocity on the diameter of the soil particle. The blue dots correspond to the correction of the threshold friction velocity from the drag partition scheme when f_{drag} is constant. **(b)** Dependence of the drag correction parameter on the aerodynamic roughness length z_o (left), and the smooth roughness length z_{os} (right).

ACPD
12, 13237–13298, 2012

New parameterization of dust emissions in EMAC

M. Astitha et al.

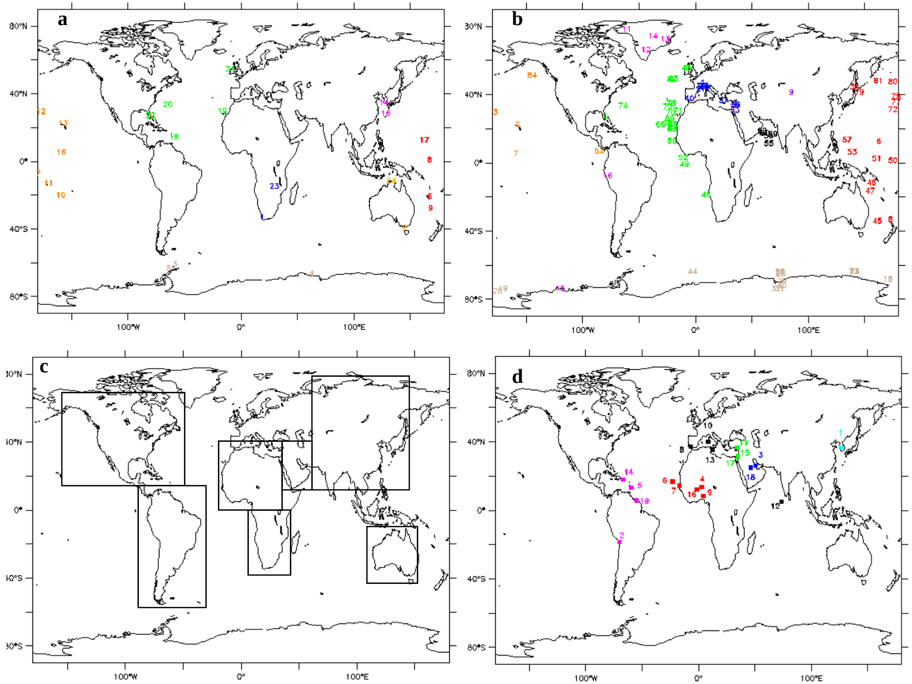

Fig. 3. Stations used for the model evaluation: **(a)** for dust concentrations, **(b)** for dust deposition. The names of the stations that correspond to each number are given in the supplement. **(c)** The black boxes denote the areas for the calculation of the regional emissions in Table 6. **(d)** Location of the 19 AERONET stations used for the model evaluation of AOD.

ACPD
12, 13237–13298, 2012

New parameterization of dust emissions in EMAC

M. Astitha et al.

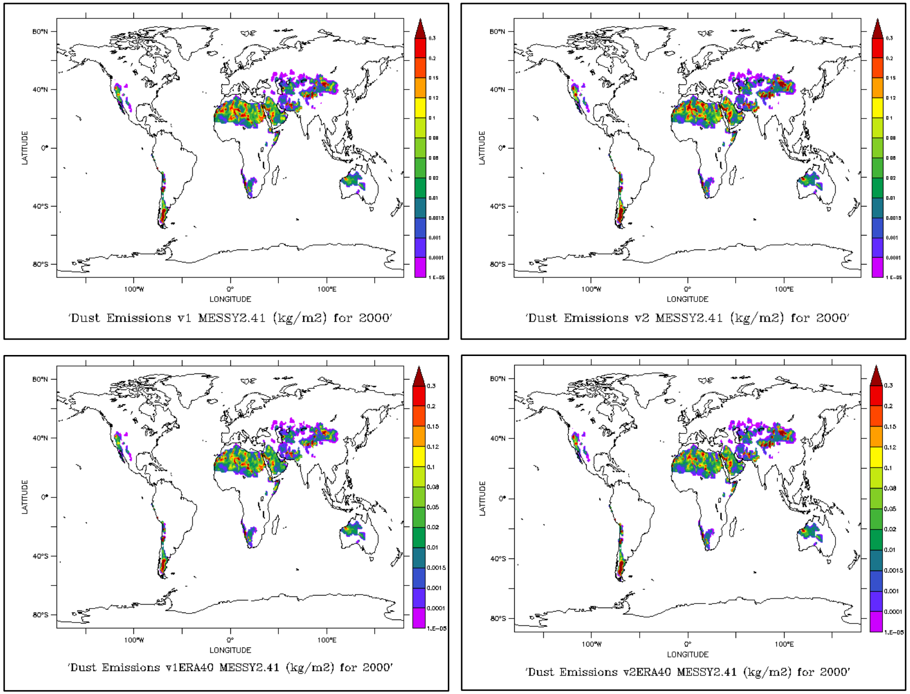

Fig. 4. Annual dust emissions (kg m^{-2}) for the year 2000: using the free-running mode with DU1 (upper left plot) and DU2 (upper right plot) schemes and using the nudged mode with DU1 (lower left plot) and DU2 (lower right plot) schemes.

ACPD
12, 13237–13298, 2012

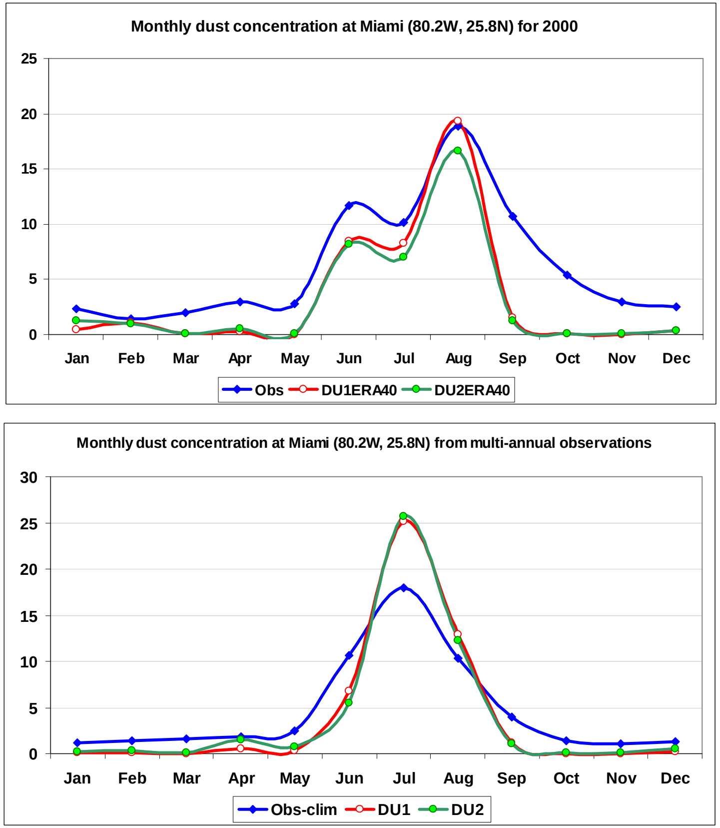

Fig. 5. Comparison of monthly modelled and measured dust concentrations ($\mu g\,m^{-3}$) at the station Miami. The upper panel shows results from the nudged simulations and the lower panel from the free-running simulation. Measurements for the year 2000 are indicated in blue line in the upper panel; the climatology of the station (multi-annual averages) is shown in blue line in the lower panel. The model results from DU1 are shown in red and from DU2 in green.

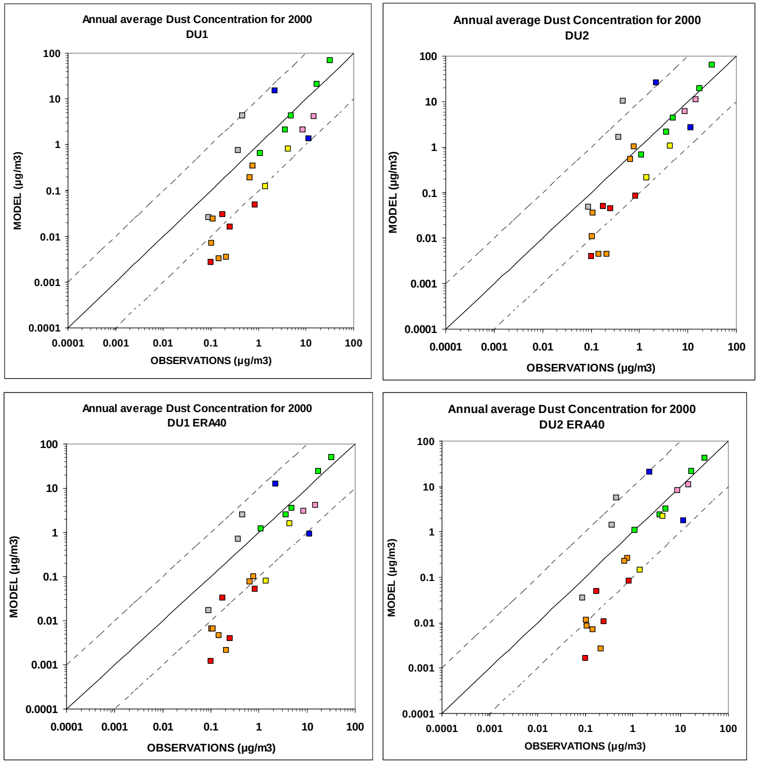

Fig. 6. Annual mean dust concentrations from the simulation of the year 2000 compared to measured multi-annual means at 24 stations. The colours correspond to the location of each station, as shown in Fig. 3a. E-Pacific = red, W-Pacific = orange, S-Africa = blue, Atlantic = green, Australia = yellow, Asia = pink, S-Ocean = grey. The dotted lines denote the 1 : 10 to 10 : 1 range.

ACPD
12, 13237–13298, 2012

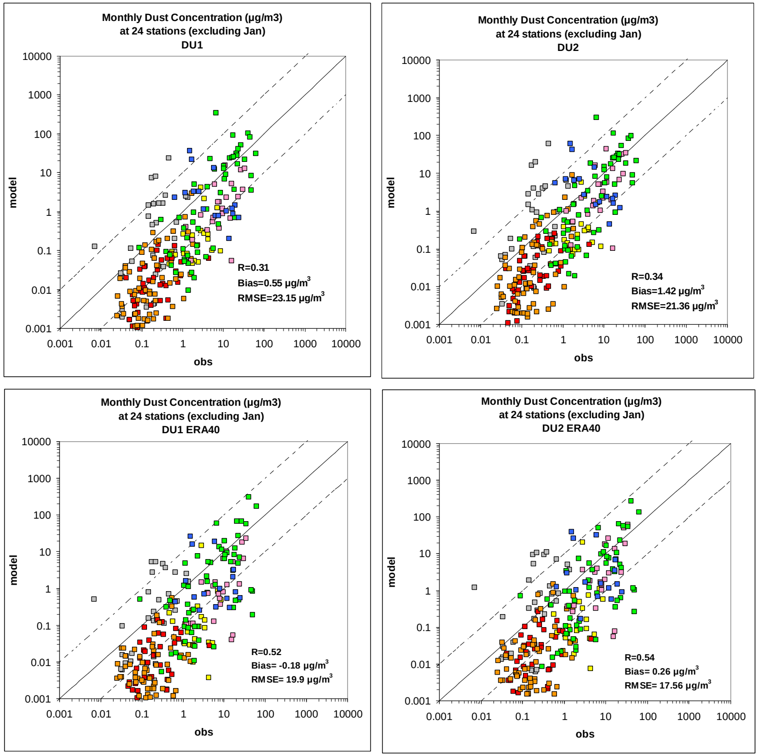

Fig. 7. Comparison of modelled monthly with measured multi-annual dust concentrations at 24 stations (January excluded). The colours correspond to the location of each station, as shown in Fig. 3a. E-Pacific = red, W-Pacific = orange, S-Africa = blue, Atlantic = green, Australia = yellow, Asia = pink, S-Ocean = grey. The dotted lines denote the 1 : 10 to 10 : 1 range.

ACPD
12, 13237–13298, 2012

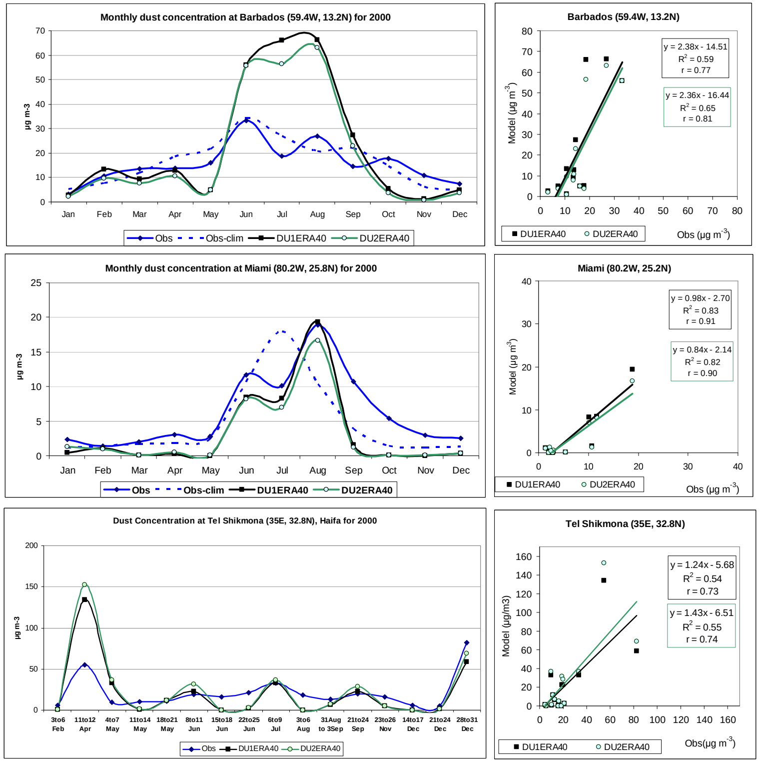

Fig. 8. Comparison of modelled and measured dust concentrations for the year 2000 for stations in Barbados (upper plot), Miami (middle plot) and Tel Skikmona, Haifa (lower plot). Measurements for the year 2000 are indicated in blue; the multi-annual average concentrations are shown by the blue dotted line. The model results from DU1 are shown in black and from DU2 in green (nudged simulations). The scatter plots on the right also list the linear regressions and correlation coefficients.

ACPD
12, 13237–13298, 2012

New parameterization of dust emissions in EMAC

M. Astitha et al.

Title Page
Abstract Introduction
Conclusions References
Tables Figures
◀ ▶
Back Close
Full Screen / Esc
Printer-friendly Version
Interactive Discussion

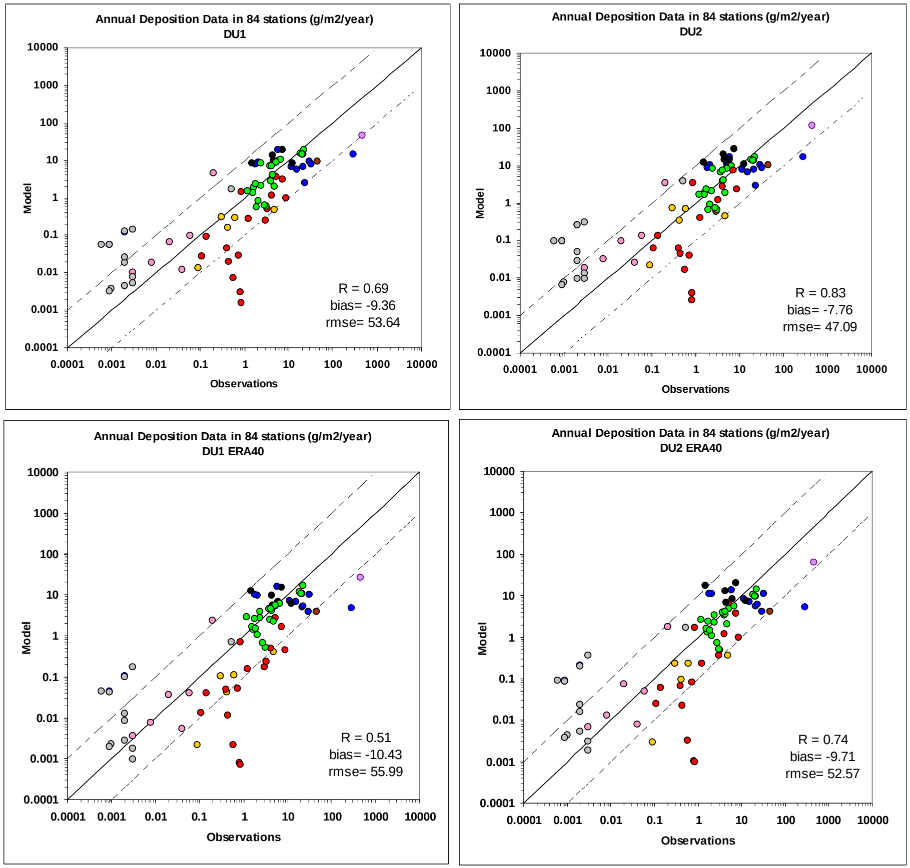

Fig. 9. Comparison of modelled and measured annual dust deposition ($g\,m^{-2}\,yr^{-1}$) from 84 stations. The stations are shown in Fig. 3b and the colour of the dots corresponds to the location of each station. E-Pacific = red, W-Pacific = orange, S-Africa = blue, Atlantic = green, Australia = yellow, Asia = pink, S-Ocean = grey. The dotted lines denote the 1 : 10 to 10 : 1 range.

ACPD
12, 13237–13298, 2012

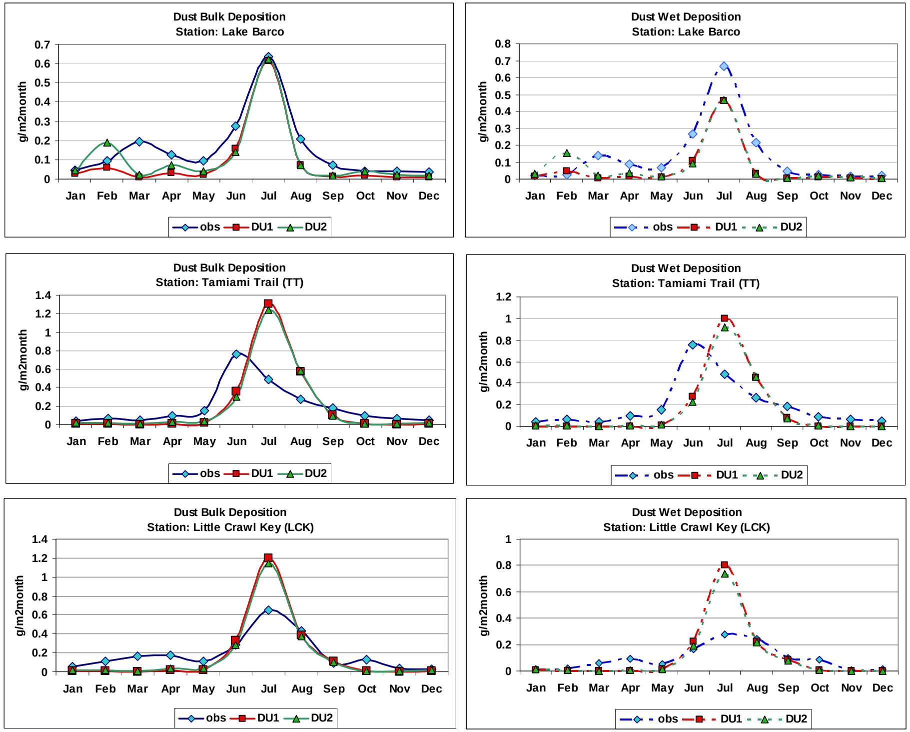

Fig. 10. Comparison of modelled and measured monthly dust deposition fluxes (g m^{-2}y^{-1}) at 3 locations in Florida (FAMS Network; measurements are provided as a 3-yr mean for 1994–1996): Lake Barco (LB) (82.02° W, 29.67° N), Tamiami Trail (TT) (80.82° W, 25.77° N) and Little Crawl Key (LCK) (80.98° W, 24.75° N). The left plots show the total deposition fluxes and the right plots the wet deposition fluxes (g m^{-2} month^{-1}).

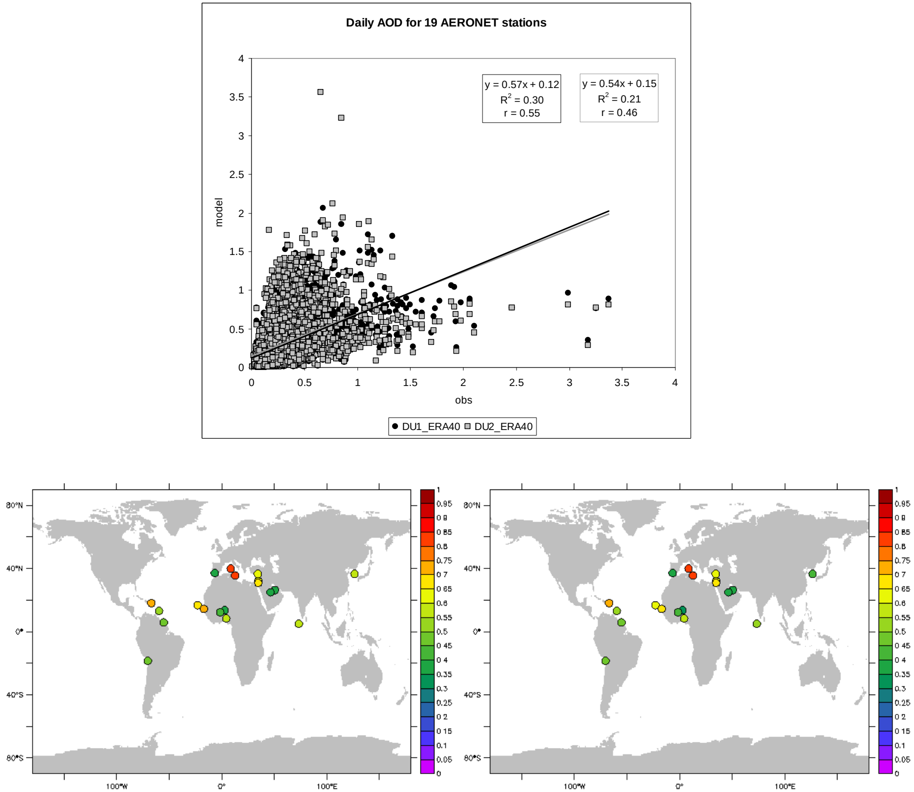

Fig. 11. Scatter plot of the modelled versus measured daily $AOD_{550\,nm}$ from the 19 AERONET stations for the DU1_ERA40 and the DU2_ERA40 simulations. The two lower panels show the correlation coefficients for each of the 19 stations for the DU1_ERA40 (left) and DU2_ERA40 (right) simulations (daily average).

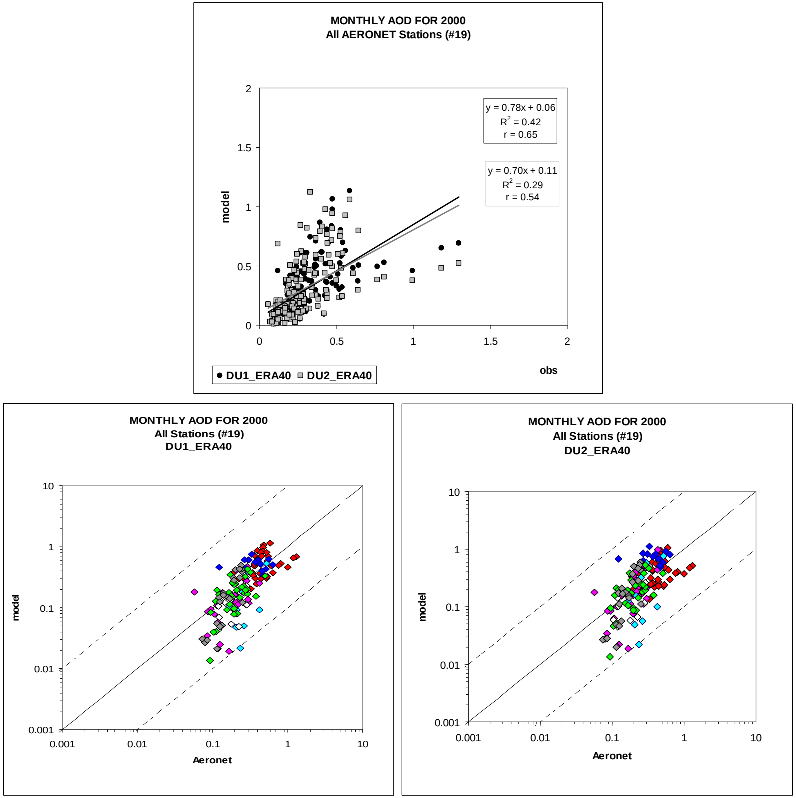

Fig. 12. Scatter plots (upper: linear, lower: logarithmic) of the modelled versus measured monthly $AOD_{550\,nm}$ from the AERONET stations for the DU1_ERA40 and the DU2_ERA40 simulations. The stations are shown in Fig. 3d and the colour of the dots corresponds to the location of each station: Africa = red, Indian Ocean and N-America = white, Europe = grey, Middle East = green, S-America = purple, Arabian Peninsula = blue. The dotted lines denote the 1 : 10 to 10 : 1 range.

ACPD
12, 13237–13298, 2012

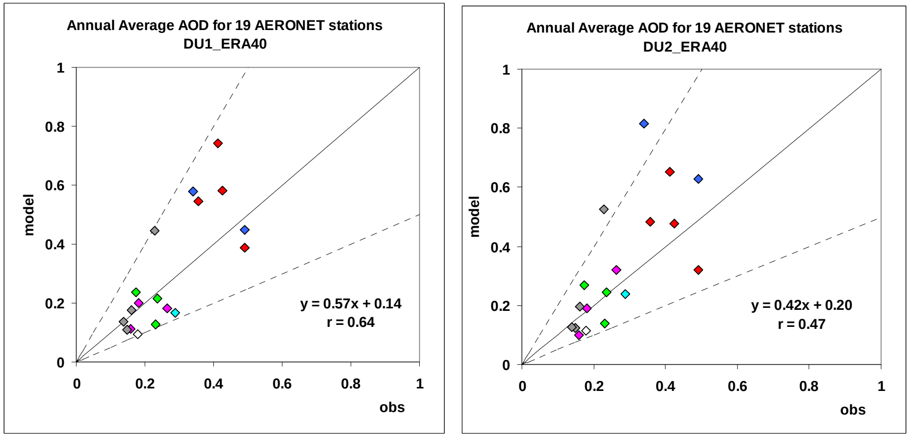

Fig. 13. Scatter plots of the modelled versus AERONET measured annual $AOD_{550\,nm}$ for the DU1_ERA40 (left plot) and for the DU2_ERA40 (right plot) simulations. The colour of the dots corresponds to the location of the stations: Africa = red, Indian Ocean and NAmerica = white, Europe = grey, Middle East = green, S-America = purple, Arabian Peninsula = blue. The dotted lines denote the 1:2 to 2:1 range.

ACPD
12, 13237–13298, 2012

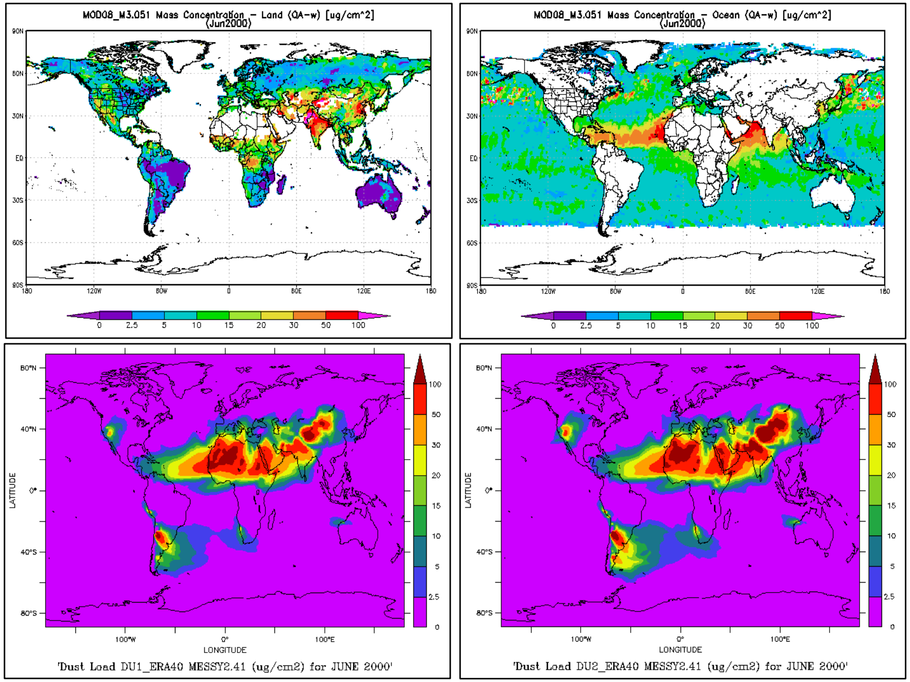

Fig. 14. Column aerosol mass concentration ($\mu g\,cm^{-2}$) from the MODIS-Terra (v5.1) satellite (upper panels) and from the model simulations using the DU1 and DU2 emissions schemes (lower panels) for June 2000.

ACPD

12, 13237–13298, 2012